# Analysis of the equilibrium wall model for high-speed turbulent flows

Prahladh S. Iyer and Mujeeb R. Malik

Phys. Rev. Fluids **4**, 074604 — Published 25 July 2019
DOI: 10.1103/PhysRevFluids.4.074604

# Analysis of the Equilibrium Wall Model for High-Speed Turbulent Flows

Prahladh S. Iyer*
*National Institute of Aerospace, Hampton, VA 23666, USA*

Mujeeb R. Malik†
*NASA Langley Research Center, Hampton, VA 23681, USA*

We perform *a priori* and *a posteriori* analyses of the equilibrium wall model for high-speed wall-bounded turbulent flows. The time-averaged flow from various DNS databases is used as input to the wall model, and the accuracy of the predictions in terms of wall shear stress and wall temperature (or heat flux for isothermal wall boundary conditions) are assessed. Two different mixing-length-based eddy viscosity models, and various damping functions are tested in this study. Both mixing-length models involve two adjustable parameters: (i) the Karman constant ($\kappa$), which varies in literature from 0.37 to 0.44, and (ii) a viscous damping constant ($A^+$ for the Van-Driest damping function). Also, for compressible flows, multiple scalings can be used for the viscous wall-normal spacing in the damping function. The sensitivity of the results to these model parameters are reported, and it is found that the predictions of skin-friction and wall temperature (or heat flux) are sensitive to the constants used, damping function scaling, and the wall model exchange location. Wall-modeled Large-Eddy Simulation (WMLES) is performed for (i) supersonic channel flow with cold wall, and (ii) axisymmetric supersonic boundary layer at adiabatic wall condition, to verify the *a priori* trends observed with respect to the damping functions. *A posteriori* WMLES results are consistent with the trends observed in the *a priori* analysis of DNS data, thus indicating the usefulness of the *a priori* analysis. We introduce a new damping function scaling, which appears to work better than existing scalings over a range of Mach numbers and thermal wall conditions.

## I. INTRODUCTION

Many practical flows are turbulent in nature, e.g., those over cars, airplanes and space vehicles; and predicting skin-friction drag and heat flux accurately are a crucial component of the design. The applications typically involve fluid flow at high Reynolds numbers (and Mach numbers for space vehicles) causing the flow to be turbulent. When using Computational Fluid Dynamics (CFD) in the design of such applications, various fidelities can be utilized depending on the available resources. Low-fidelity Reynolds-Averaged Navier-Stokes (RANS) models involve modeling all of the turbulence, and solving only for the time-averaged flow quantities. While computationally efficient, it suffers in accuracy for complex flows. Higher-fidelity scale-resolving methods such as Large Eddy Simulation (LES), and Direct Numerical Simulation (DNS) are quite accurate but are computationally very expensive, especially for practical applications. Spalart et al. [1] estimate that an LES of an aircraft wing at flight $Re$ (10 million based on the chord) would require on the order of 100 billion grid points (assuming a modest 20 points per boundary layer thickness) and 5 million time steps, and thus, wall-resolved LES of a full aircraft configuration would not be feasible for the foreseeable future.

The wall-modeled LES approach, in which the near-wall region is modeled with RANS, while the majority of the length scales away from the wall are resolved using LES, is a reasonable compromise between accuracy and computational cost. Wall-modeled LES can further be classified into (i) Stress-based WMLES, and (ii) hybrid RANS/LES methods such as Improved Delayed Detached Eddy Simulation (IDDES). In the stress-based WMLES approach, the computational grid is coarse in the wall-normal (and wall-parallel) direction, thus requiring the regular no-slip boundary condition to be supplemented by a wall shear stress (and heat flux/ temperature) boundary condition. See Cabot & Moin [2], Piomelli & Balaras [3], Larsson et al. [4] and Bose & Park [5] for overviews of stress-based WMLES. In IDDES, the grid is very fine in the wall-normal direction but coarse in the wall-parallel direction thus requiring the LES eddy viscosity to be replaced by a RANS eddy viscosity where the majority of the turbulence is modeled. See Spalart [6], Deck [7], Spalart et al. [8] and Shur et al. [9] for an overview of the DES-based approach. In this study, we focus on the stress-based WMLES approach, which is implied when we refer to WMLES in the rest of the manuscript.

---

* prahladh.iyer@nianet.org
† mujeeb.r.malik@nasa.gov

Stress-based WMLES can be further classified into equilibrium and nonequilibrium models depending on the level of complexity of the wall model. The equilibrium wall model neglects nonequilibrium effects such as acceleration and pressure gradient, and works quite well for canonical wall-bounded flows such as channels and boundary layers. The relatively simple zero-equation mixing-length model for the eddy viscosity has been widely used in WMLES of wall-bounded turbulent flows (channel, boundary layers and Couette flow) with reasonable success. Note that the mixing-length model involves two empirical constants for incompressible speeds, namely the von Karman constant ($\kappa$), and the damping function constant ($A^+$ for the Van-Driest function). For low-speed flows, the definition of $y^+ = yu_\tau/\nu$ in the damping function is unambiguous, whereas for high-speed flows, the wall-normal co-ordinate ($y$) can be non-dimensionalized (to $y^+$) by either using the wall properties (density and viscosity), local properties or a combination of both. While WMLES has performed well for low-speed flows [2, 3], its application to high-speed flows is more recent [10–13] and has been limited in terms of the range of Mach number, and thermal wall condition simulated. Note that high-fidelity DNS/LES data itself is scarce as compared to the incompressible flow regime.

There is limited freedom to change the scalings used in the eddy viscosity model, as the compressible law of the wall relation fixes the scaling used for the eddy viscosity in the log-layer. However, the damping function, which was first introduced by Van-Driest [14] for low-speed flows, is purely empirical with its constant ($A^+$) set to match the correct intercept of the log-law. For compressible flows, multiple normalizations ($y^+$) of the wall-normal coordinate ($y$) are possible, which is the main focus of this study. This has been previously investigated in the context of $k-\epsilon$ RANS model by Aupoix & Viola [15]. They determined that the semilocal scaling yields best results overall. In the context of WMLES with an equilibrium wall model, Kawai & Larsson [10] used the wall scaling for the damping function. Bocquet et al. [11] and Yang & Lv [16] compared the wall and semilocal scalings and found that the semilocal scaling works best. However, both the aforementioned studies only investigated flows with cold-wall thermal boundary conditions.

In this study, we assess the performance of the equilibrium wall model with a mixing-length type eddy-viscosity model and different damping function scalings for the Van-Driest damping function, over a range of thermal boundary conditions (from adiabatic to cold wall) and Mach numbers matching available DNS databases. Note that this study does not deal with errors associated with the log-layer mismatch, and uses the fix proposed by Kawai & Larsson[10] to minimize such errors in the *a posteriori* WMLES simulations. *A priori* analysis is performed with existing and new damping function scalings, and the errors in predicting the wall quantities (skin friction and temperature/heat flux) are reported at various exchange locations from which data is input to the wall model. We empirically determine a wall-normal scaling for the Van-Driest damping function that appears to work best over a range of Mach numbers and thermal conditions. We also examine the sensitivity of the predictions to different mixing length models, inclusion of pressure gradient effects and turbulent Prandtl number. Finally, *a posteriori* WMLES are performed for two flow conditions: (i) Mach 3 channel flow with a cold wall, and (ii) Mach 2.85 axisymmetric turbulent boundary layer with an adiabatic wall, to test the consistency of the effect of damping function scaling from the *a priori* analysis.

This paper is organized as follows. The equilibrium wall model equations along with the eddy viscosity models and damping functions are described in Section II. Results from the *a priori* analysis of the wall model are reported along with sensitivity to various parameters in Section III. The *a posteriori* WMLES results are reported for the supersonic channel and axisymmetric boundary layer in Section IV, and the main findings are summarized in Section V.

## II. EQUILIBRIUM WALL MODEL

The equilibrium wall model equations are derived from the compressible Reynolds-Averaged Navier-Stokes equations with the boundary layer approximation, and neglecting nonequilibrium terms such as pressure gradient, as given below:

$$\frac{\mathrm{d}}{\mathrm{d}y}[(\mu+\mu_t)\frac{\mathrm{d}u}{\mathrm{d}y}] = 0 \tag{1}$$

$$\frac{\mathrm{d}}{\mathrm{d}y}[(\mu+\mu_t)u\frac{\mathrm{d}u}{\mathrm{d}y} + (k+k_t)\frac{\mathrm{d}T}{\mathrm{d}y}] = 0 \tag{2}$$

Here, $y$ is the wall-normal coordinate, $u$ is the mean wall-parallel velocity magnitude, $T$ is the mean temperature, $\mu$ and $k$ are the mean dynamic viscosity and thermal conductivity and $\mu_t$ and $k_t$ are the eddy viscosity and turbulent thermal conductivity, respectively. In the above equations, $y$ and $u$ are defined with reference to the corresponding wall values (i.e., $y = u = 0$ at the wall). More details of the equilibrium wall model can be found in Larsson et al. [4]. The eddy viscosity can be defined as following:

$$\mu_{t,JK} = \rho \kappa y \sqrt{\tau_w/\rho} D \tag{3}$$
$$\mu_{t,Pr} = \rho \kappa^2 y^2 |du/dy| D \tag{4}$$

The eddy viscosity for the wall model is obtained from the mixing-length model in which the length scale is taken to be $\kappa y$, while the velocity scale is either taken to be the local friction velocity ($u_\tau^* = \sqrt{\tau_w/\rho}$) or the length-scale multiplied by the velocity gradient ($\kappa y \frac{\partial u}{\partial y}$) as shown in Equation 4. Here, $\kappa$ is the von Karman constant taken to be 0.41 in this study, but varies in literature between 0.37 and 0.44. The sensitivity of the predictions to $\kappa$ is small, as discussed in Section III. The eddy viscosity/ conductivity is multiplied by a damping function $D$ to ensure that $\mu \gg \mu_t$ close to the wall. Note that the expression for eddy viscosity in Equation 3 is of the same form as the Johnson-King model [17] and so, following Cabot [18], who appears to be the first to use this model, the subscript JK is used. The expression in Equation 4 is based on the work of Prandtl [19] and so the subscript Pr is used. The eddy conductivity is computed from the eddy viscosity and specific heat of the gas ($C_p$), assuming a constant turbulent Prandtl number ($Pr_t$) as follows:

$$k_t = \frac{C_p \mu_t}{Pr_t} \tag{5}$$

In the region beyond the buffer layer, typically for $y^+ \gtrsim 30$ (log-law region), the turbulent stresses dominate over the viscous stresses ($\mu_t \gg \mu$), and so for large $y^+$, the damping function ($D$) is designed to be unity (since no damping is necessary). Under these conditions, integrating the momentum equation (Equation 1) with respect to $y$ reduces to:

$$\mu_t \frac{\mathrm{d}u}{\mathrm{d}y} = \tau_w = \rho_w u_\tau^2 \tag{6}$$

Substituting the JK and Pr mixing length models, and setting $u_\tau = \sqrt{\tau_w/\rho_w}$, we obtain:

$$\mu_{t,JK} \frac{\mathrm{d}u}{\mathrm{d}y} = \rho_w u_\tau^2 \implies \kappa y \frac{\mathrm{d}u}{\mathrm{d}y} = \sqrt{\frac{\rho_w}{\rho}} u_\tau \tag{7}$$
$$\mu_{t,Pr} \frac{\mathrm{d}u}{\mathrm{d}y} = \rho_w u_\tau^2 \implies (\kappa y)^2 |\frac{\mathrm{d}u}{\mathrm{d}y}|^2 = \frac{\rho_w}{\rho} u_\tau^2 \tag{8}$$

It is straightforward to see that Equations 7 and 8 are identical, with the Prandtl mixing length model giving square of the equation obtained using the JK mixing length model. This is the familiar compressible law of the wall relationship (Van-Driest [20], Bradshaw [21], Huang et al. [22]). Thus, both the mixing-length models seem to be appropriate as they reduce to the compressible law of the wall.

We now turn our attention to the damping function ($D$). The most popular damping function is the one given by Van-Driest [14] (VD). In this study, we also examine the damping function used in the popular Spalart-Allmaras [23] (SA) RANS model which is in turn based on the work of Mellor & Herring [24], and a modified VD damping function proposed by Piomelli et al. [25]. Note that all the damping functions are empirical in nature with constants tuned to yield proper decay of the eddy viscosity for small $y^+$. The damping functions are given below:

$$D_{VD} = [1 - \exp(-\frac{y^+}{A^+})]^2 \tag{9}$$
$$D_{SA} = \frac{\hat{\mu}_t^3}{(\hat{\mu}_t^3 + C_{v1}^3 \mu^3)} \tag{10}$$
$$D_{Pio} = [1 - \exp[-(\frac{y^+}{A^+})^3] \tag{11}$$

While the Van-Driest and Piomelli et al. [25] damping functions depend on the nondimensionalized wall-normal distance ($y^+$), the Spalart-Allmaras damping function depends on the undamped eddy viscosity ($\hat{\mu}_t$) and dynamic viscosity ($\mu$). Note that all three are empirical in nature, with corresponding empirical constants $A^+$ and $C_{v1}$. The main requirement of the damping function is that $D \approx 1$ for $y^+ \gtrsim 30$, and $D \to 0$ for $y^+ \to 0$, typically as $y^2$ or $y^3$. The constant $A^+$ is chosen to match the intercept in the log-law region of the velocity profile and is found to be 26 [14] for the Prandtl mixing-length model, and 17 for the Johnson-King based mixing-length model when using the Van-Driest damping function. The sensitivity of the results to $A^+$ is reported in Section III. For constant density incompressible flows, there is no ambiguity in defining $y^+ = yu_\tau/\nu$; however, for compressible flows, multiple definitions are possible depending on whether we choose the local density/ viscosity or the corresponding wall values. Note that for the SA damping function, $C_{v1} = 7.1$ and the local viscosity is used for compressible flows.

### A. Damping Function Scalings

If we define the wall friction velocity, $u_\tau = \sqrt{\tau_w/\rho_w}$, and the local friction velocity as $u_\tau^* = \sqrt{\tau_w/\rho}$, multiple definitions of $y^+$ used in the Van-Driest damping function are possible, with two listed below:

$$
\begin{aligned}
y^+_{wall} &= \frac{\rho_w u_\tau y}{\mu_w} \\
y^+_{SL} &= \frac{\rho u_\tau^* y}{\mu} = \frac{\sqrt{\rho\rho_w} u_\tau y}{\mu}
\end{aligned}
$$

The wall and semilocal (SL) scalings have previously been used in the WMLES literature. For high-speed flows, the wall scaling has been used by Kawai & Larsson [10], Bermejo-Moreno et al. [12], among others, while the semilocal scaling has been used by Bocquet et al. [11] and more recently by Yang & Lv [16]. Bocquet et al. [11] simulated the cold wall Mach 3 channel flow corresponding to the DNS of Coleman et al. [26] (also used in this study), and found that the semilocal scaling gives improved predictions when compared to the wall scaling. Yang & Lv [16] studied the cold wall supersonic Couette flow case, and found that with the wall scalings, the error in prediction of $C_f$ can be of the order of 100% for large Mach numbers. They however did not report the errors in the prediction of wall heat flux. The semilocal scaling and the eddy-viscosity form used in Equation 3 can be derived from the Trettel-Larsson transformation [27] to collapse compressibility effects (see [16]). Since the Trettel-Larsson transformation was quite successful in collapsing the compressible velocity profiles to the corresponding incompressible ones (especially for cold wall flows), one might expect that the semilocal scaling would be very accurate. However, our results suggest that this may not be the case. Also, more recently, Zhang et al. [28] reported that the Trettel-Larsson transformation is less successful than previously observed ([27, 29]) based on their DNS of hypersonic turbulent boundary layers. In the absence of an "exact" compressible transformation, it is worth looking into other empirical scalings. In this study, we propose additional scalings as shown below:

$$
\begin{aligned}
y^+_{local} &= \frac{\rho u_\tau y}{\mu} \\
y^+_{mixed} &= \frac{(y^+_{wall} + y^+_{SL})}{2} \\
y^+_{mixed2} &= \frac{(y^+_{local} + y^+_{SL})}{2} \\
y^+_{mixedmin} &= \min(y^+_{mixed}, y^+_{SL}) \\
y^+_{mixedmin2} &= \min(y^+_{mixed}, y^+_{mixed2})
\end{aligned}
$$

The local scaling uses the local properties and $u_\tau$ instead of $u_\tau^*$ used in the semilocal scaling. The mixed scaling is a simple average of the wall and semilocal scalings, while the mixed2 scaling is the simple average of the local and semilocal scalings. The mixedmin scaling uses the minimum of the mixed and semilocal scalings, while the mixedmin2 scaling uses the minimum of the mixed and mixed2 scalings. It will be seen later that the mixed scaling works best at adiabatic conditions, while the semilocal or mixed2 scaling works best for most of the cold wall flows considered in this study. For adiabatic flows, $T(y) < T_w$, and thus $y^+_{wall} < y^+_{SL}$ implying that $y^+_{mixed} < y^+_{SL}$. Similar reasoning for cold wall flows implies that $y^+_{mixed} > y^+_{SL}$. Thus, the mixedmin scaling uses the minimum of the mixed and SL scalings so that it is identical to the mixed scaling for hot walls, and to the semilocal scaling for cold walls. The mixedmin2 uses the same rationale but instead switches to the mixed2 scaling for cold walls. Note that all the compressible scalings obey the basic requirements of a damping function ($D \to 0$ as $y \to 0$, and $D \approx 1$ for $y^+ \gtrsim 30$), and reduce to the same $y^+ = yu_\tau/\nu$ for constant density incompressible flows. It should be noted that since the damping function itself is purely empirical and adjusted to yield the correct near-wall eddy viscosity behavior, it appears that the choice of a suitable damping function scaling for high-speed flows must also be determined empirically.

### B. Solution of Wall-Model Equations

The wall model equations listed in Equations 1-5 are solved using information from the LES solution (for a WMLES) or the DNS/ LES database (for *a priori* analysis) at a certain distance from the wall, and returns the wall shear stress and heat flux (or wall temperature for adiabatic flows). A second-order staggered finite-difference scheme is used to solve the coupled system of equations. For the WMLES, the quantities returned by the wall model are applied as a boundary condition to the LES near-wall grid point after solving the coupled Ordinary Differential Equations (ODE). In all the results reported, 41 grid points were used with the first grid point spacing of $\Delta y^+ < 0.1$. Further increase in grid points did not significantly alter the results. The equations were solved until a maximum residual of $10^{-8}$ was reached for both $u/u_\infty$ and $T/T_\infty$ up to a maximum of 1000 iterations. Preliminary tests were used to determine the number of grid points, number of iterations and residual that give acceptably good grid converged results. The wall model code was also validated with the *a priori* results of Bocquet et al. [11] for the cold-wall channel flows, and excellent agreement was obtained. Further details about the wall model and implementation can be found in Kawai & Larsson [10] and Larsson et al. [4].

Historically, in WMLES, the solution from the first grid point adjacent to the wall was used as input to the wall model, but Kawai & Larsson [10] showed that the LES solution in the first few grid points is inherently erroneous. Most studies have thus chosen an exchange location of $\approx 5-10\%$ of the boundary layer thickness ($\delta_{99}$) or half-width ($h$) for channel flows, with at least 3 grid points between the wall the exchange location. One of the objectives of this study is to determine a suitable exchange location for a range of flow conditions.

For the *a priori* analysis, DNS data is input to the wall-model equations at different distances from the wall, and the outputs of the wall model are compared to the corresponding values from DNS. The wall skin friction ($C_f$) and heat transfer parameter ($B_q$) for isothermal flows are defined as:

$$C_f = \frac{\mu \frac{\mathrm{d}u}{\mathrm{d}y}|_w}{\frac{1}{2}\rho_\infty u_\infty^2} \tag{12}$$

$$B_q = \frac{-k\frac{\mathrm{d}T}{\mathrm{d}y}|_w}{\rho_w u_\tau C_p T_w} \tag{13}$$

The error ($\varepsilon_Q$) in any wall model output quantity ($Q$) is defined as:

$$\varepsilon_Q(\%) = (\frac{Q_{wm} - Q_{DNS}}{Q_{DNS}}) \times 100\% \tag{14}$$

Here, $Q$ is either $C_f$, or $B_q$ for isothermal walls and $T_w$ for adiabatic walls. Note that the error ($\varepsilon_Q$) is independent of the sign convention used for any quantity ($Q$) such as $B_q$.

## III. *A PRIORI* ANALYSIS OF DNS DATA

For the *a priori* analysis, publicly available turbulent DNS databases[1] are used in this study as listed below:

- Incompressible channel database for $Re_\tau \approx 590$ flow corresponding to Moser et al. [30] [`http://turbulence.ices.utexas.edu/data/MKM/chan590/`], and $Re_\tau \approx 2000$ flow corresponding to Lee & Moser [31] [`http://turbulence.ices.utexas.edu/channel2015/content/Data_2015_2000.html`].
- Incompressible boundary layer database upto $Re_\theta = 8300$ corresponding to Eitel-Amor et al. [32] [`ftp://ftp.mech.kth.se/pub/pschlatt/DATA/TBL/SIM/RE8000/`].
- Supersonic channel database at Mach 1.5 and 3 and cold wall conditions corresponding to the study of Coleman et al. [26] [`https://turbmodels.larc.nasa.gov/Other_DNS_Data/supersonic-channel.html`], and Modesti & Pirozzoli [29][`http://newton.dima.uniroma1.it/supchan/`].
- Supersonic turbulent boundary layer database from Mach 2 to 4 corresponding to the study of Pirozzoli & Bernardini [33, 34] and Bernardini & Pirozzoli [35, 36] [`http://reynolds.dma.uniroma1.it/dnsm2/stat/`] at adiabatic conditions.

[1] Last accessed: January 10, 2019

- Supersonic/ hypersonic turbulent boundary layer database corresponding to the study of Zhang et al. [28] [`https://turbmodels.larc.nasa.gov/Other_DNS_Data/supersonic_hypersonic_flatplate.html`] over a range of thermal conditions.

### A. Incompressible Flows

We first assess the accuracy of the wall model for incompressible flows and its sensitivity to various parameters before considering compressible flows. Since high-quality pseudospectral DNS results are available for the turbulent channel flow, we choose to assess the sensitivities for this flow. We will then check the findings for a lower Reynolds number channel and a turbulent boundary layer. The temperature is assumed to be constant, and the energy equation (Equation 2) is not solved for the results in this section.

#### 1. $Re_\tau \approx 2000$ *turbulent channel: Sensitivity To Various Parameters*

We examine the sensitivity of the wall model to the mixing-length model, damping constant ($A^+$), von Karman constant ($\kappa$), including d$p$/d$x$ and different damping functions. We consider the $Re_\tau = 1995$ channel flow corresponding to the DNS of Lee & Moser [31] for this analysis.

The sensitivity of the predictions to the empirical constant $A^+$ used in the Van Driest damping function (Equation 9) is shown in Figure 1 for the two mixing-length models (Equations 3 and 4). The typical value of $A^+$ used for the JK model by Cabot [18] and Cabot & Moin [2] is 17, while it is 26 for the Prandtl model by Van Driest [14]. Although most studies use the aforementioned values of $A^+$ with a variation of +/- 2, we intentionally choose a broader range of $A^+$ to understand how the errors vary with $A^+$. Hence, we look at the sensitivity to $A^+$ between 10 and 25 for the JK model, and between 20 and 30 for the Prandtl model. For the results in Figure 1 and the rest of the figures in this manuscript, the abscissa is the wall normal distance from the wall at which velocity (and temperature for compressible flows) was input to the wall model (i.e., exchange location). Typically in WMLES studies, an exchange location ($y/h$) between 0.05 and 0.15 is used. Therefore, in this and following plots, this region should be the region of focus. The distance from the wall is specified in outer units (bottom axis), and viscous wall units (top axis). The error in the output quantity ($C_f$) defined by Equation 14 is the ordinate of the figure. The results from Figure 1 indicate that the wall model is highly sensitive to the value of $A^+$ for both the mixing-length models and the the lowest error is obtained with $A^+ = 17$ for the JK model and $A^+ = 26$ for the Prandtl model, consistent with previous studies. A higher value of $A^+$, which implies a lower $y^+/A^+$ and more damping, leads to a lower value of $C_f$, and vice versa. It is also evident that the value of $A^+$ is sensitive to the mixing-length model. For both models, the error in prediction (for the optimal value of $A^+$) is within 3% of the DNS value until $y/h \approx 0.15$. While the equilibrium wall model equations are technically only valid in the inner layer ($y/h$ <0.15), it can be seen that the errors are still within 5% for these two values of $A^+$ until $y/h \approx 0.5$. The other inference is that the performance of the two mixing length models are equivalent in spite of the fact that the Prandtl model uses a more local velocity scale ($\kappa y$du/dy), and so we will focus more on the JK model hereafter.

The effect of the von Karman constant ($\kappa$) on the predictions using the JK model and Van Driest damping function (with $A^+ = 17$) is shown in Figure 2(a) with $\kappa$ varying between 0.38 and 0.44. It can be seen that there is some sensitivity ($\approx 5\%$) to the value of $\kappa$. Overall, $\kappa = 0.41$ yields the best results in spite of the fact that the value of $\kappa$ obtained from DNS data by Lee & Moser [31], and others [37] was $\approx 0.384$ for channel flow at this Reynolds number. We think that this is because the value of $\kappa$ and $A^+$ together determine the overall predictive error; and for $A^+ = 17$, a corresponding value of $\kappa = 0.41$ yields the best results. Since we are using the equilibrium model which neglects the pressure gradient term (dp/dx), it is of interest to see if including this term improves the predictions. We know for a fully developed channel flow that dp/dx $= -\tau_\mathrm{w}/$h. We impose the dp/dx from DNS to the right hand side of the wall model equations (Equation 2). The Johnson-King model (with $A^+ = 17$) and the Prandtl model (with $A^+ = 26$) are considered using $\kappa = 0.41$. The results in Figure 2(b) show that including the $dp/dx$ term does not significantly improve the predictions, but rather makes the predictions worse for $y/h > 0.1$, possibly because the zero-equation eddy viscosity models used do not incorporate nonequilibrium effects. For $y/h < 0.1$, we see that the effect of $dp/dx$ is relatively small, indicating that the equilibrium assumption is reasonable very near the wall. Thus, henceforth even though we report errors until $y/h = 0.5$, we will mainly focus on the results for $y/h <= 0.1$ so that the nonequilibrium terms can be neglected in the wall model.

We compare the predictions of different mixing length models and damping functions in Figure 3. The JK model with VD ($A^+ = 17$) and SA damping functions, and Prandtl model with VD ($A^+ = 26$) and Piomelli et al. [25] damping function ($A^+ = 25$) results are shown. Overall, all the damping functions perform well for an exchange

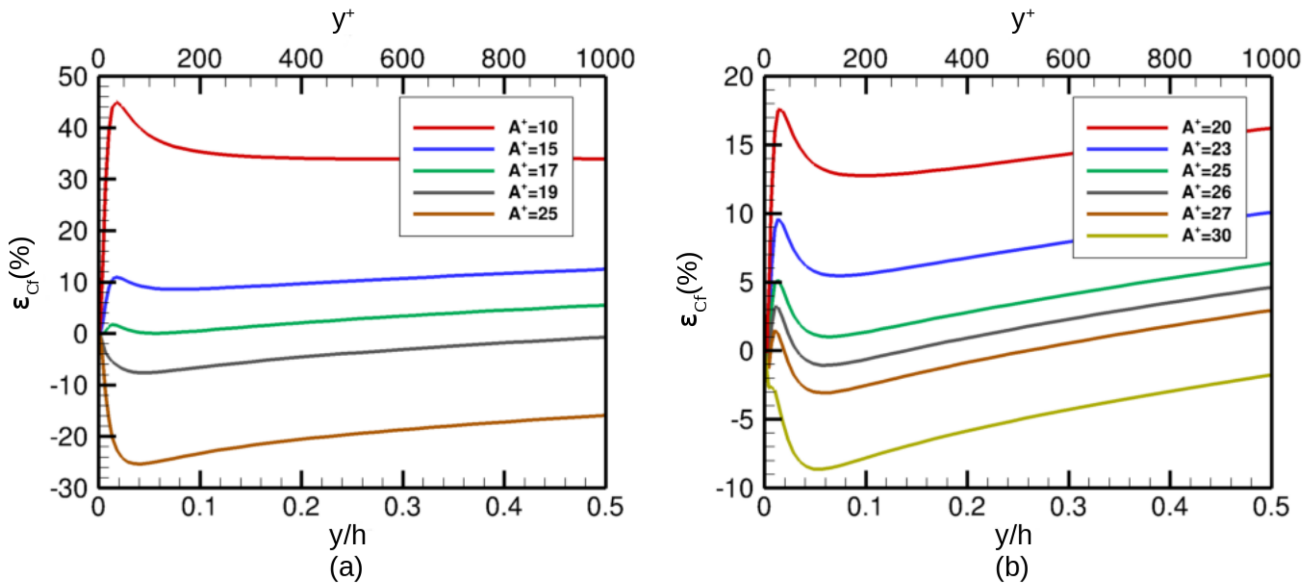


FIG. 1. The effect of the empirical constant ($A^+$) on the wall model predictions for $Re_\tau \approx 2000$ channel: (a) Johnson-King type mixing length model, (b) Prandtl mixing length model. In this and following plots, the abscissa is the exchange location at which data was input to the wall model.

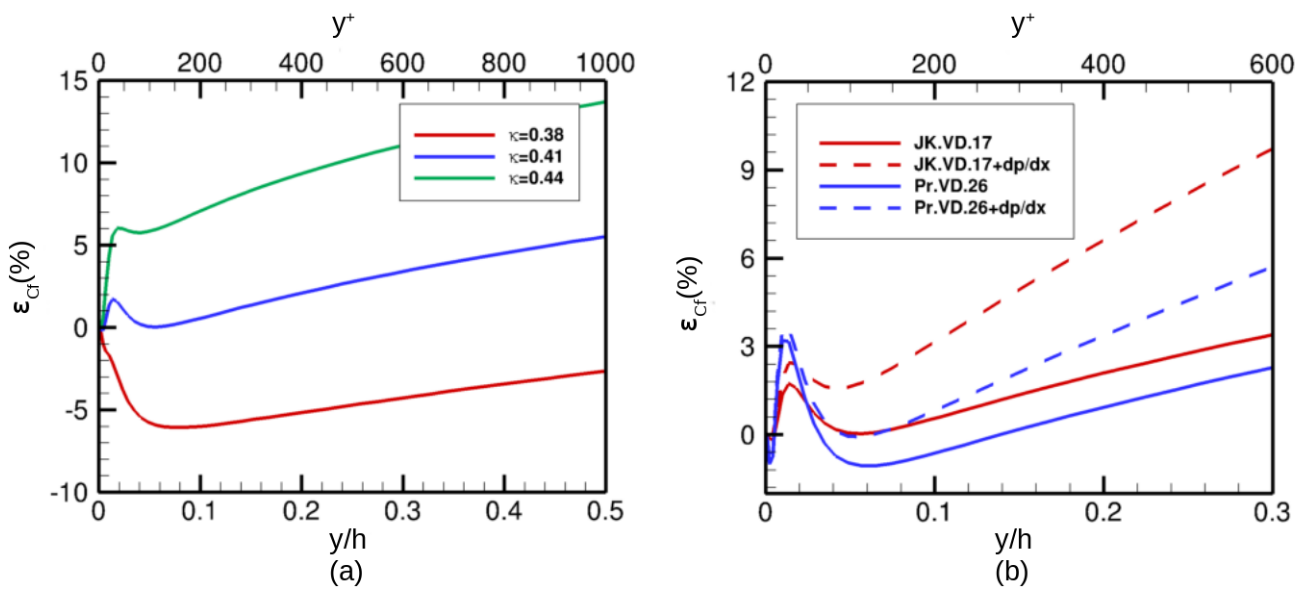


FIG. 2. The effect of (a) the von Karman constant, $\kappa$ using the Johnson-King type mixing length model, and (b) including the pressure gradient term on the wall model predictions with $\kappa = 0.41$ for both the Johnson-King ($A^+ = 17$) and Prandtl ($A^+ = 26$) models, for the $Re_\tau \approx 2000$ channel.

location ($y/h$) between 0.05 and 0.15 with under 3% error. However at locations closer to the wall ($y/h \approx 0.01$), the SA and Piomelli et al. [25] damping functions have an error up to 8% in magnitude.

### *2. $Re_\tau \approx 590$ Channel and $Re_\tau \approx 2118$ Boundary Layer*

The results for the $Re_\tau \approx 2000$ channel flow have shown that the JK and Prandtl models with VD or SA (for JK) damping functions work quite well and produce an error of less than 3% when the exchange location ($y/h$) is

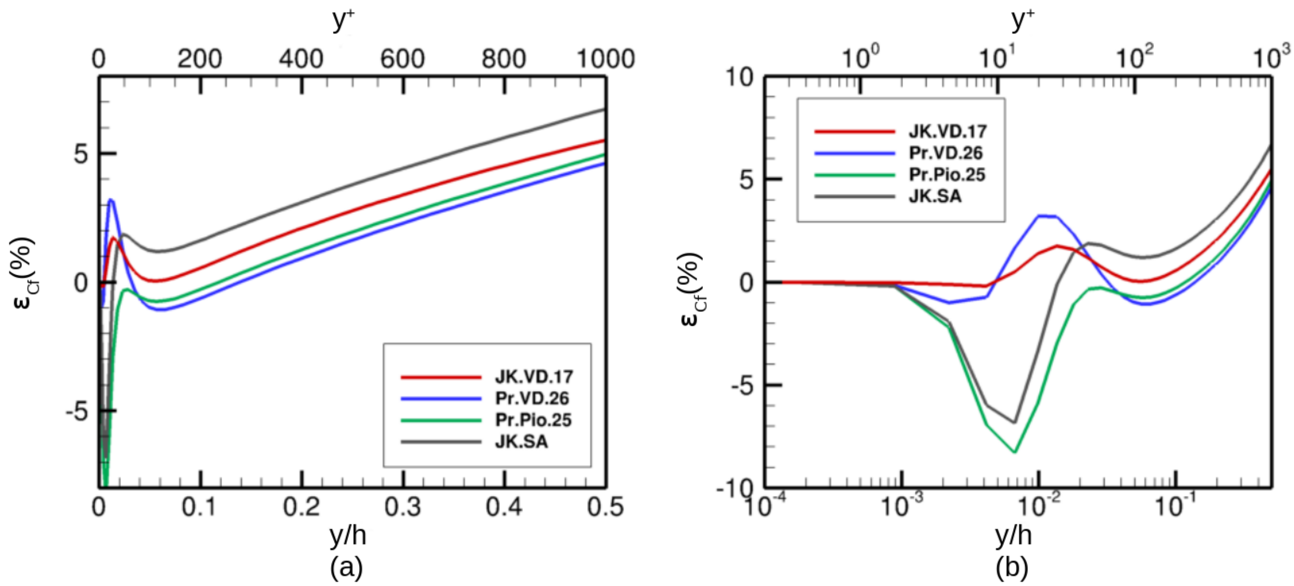


FIG. 3. Effect of different mixing length models and damping functions on the wall model predictions for $Re_\tau \approx 2000$ channel with a (a) linear scale, and (b) semi-log scaled abscissa. The numbers in the legend indicate the value of $A^+$ used in the damping function.

between 0.05 and 0.15. We now check the performance for a lower $Re$ channel at $Re_\tau \approx 590$ corresponding to the results of Moser et al. [30] and a zero pressure gradient boundary layer at $Re_\tau \approx 2118$ corresponding to the results of Eitel-Amor et al. [32] The same mixing length models for eddy viscosity and damping functions as Figure 3 are used here. The results shown in Figure 4 are consistent with those for the $Re_\tau \approx 2000$ flow. For an exchange location between 0.05 and 0.15 ($y/h$ for channel, and $y/\delta_{99}$ for the boundary layer), the error in skin friction is less than $\approx 3\%$ in magnitude for both the flows. Based on these results we can be fairly confident of the accuracy of the equilibrium wall model predictions for incompressible flows with the chosen set of parameters ($\kappa$ and $A^+$).

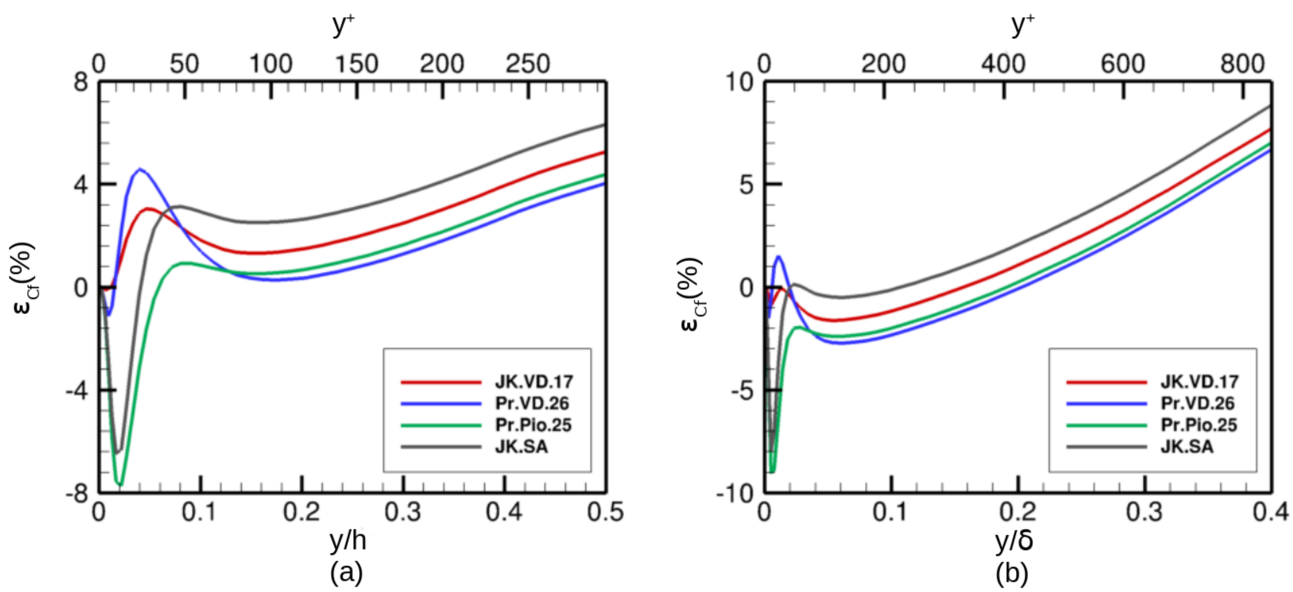


FIG. 4. Effect of different mixing length models and damping functions on the wall model predictions for (a) $Re_\tau = 590$ channel, and (b) $Re_\tau = 2118$ turbulent boundary layer.

### B. Compressible Flows

We now perform *a priori* analysis for high-speed compressible turbulent flows. We consider a cold wall supersonic channel flow, adiabatic supersonic boundary layer, and supersonic-through-hypersonic boundary layer over a range of thermal boundary conditions. The time-averaged velocity and temperature at different exchange locations are input to the wall model, and the error in the skin friction ($C_f$) and heat-transfer parameter ($B_q$) or wall temperature ($T_w$) are analyzed. Since we have already checked the sensitivity of the model to $A^+$, $\kappa$, dp/dx and mixing length model for incompressible flows, we will mainly focus on the effect of the Van Driest damping function scaling for the JK mixing-length model. We also report the results using the SA damping function since it is widely used for high-speed RANS. For a subset of cases, we will also examine the sensitivity to the mixing-length model and turbulent Prandtl number ($Pr_t$).

For the results that follow, the top horizontal axis of the figure is the viscous wall scaling $y^+ = yu_\tau/\nu_w$, with $u_\tau = \sqrt{\tau_w/\rho_w}$. The standard parameters from incompressible flow is also used here, namely $\kappa = 0.41$, $A^+ = 17$ (for JK model), and dp/dx is neglected for channel flows. Also, $Pr_t = 0.9$ for all the results reported, even though the DNS at times predicts a somewhat different value. The viscosity-temperature relationship is chosen to match the DNS simulation using either a power law or Sutherland's Law. Our tests indicated that having a different viscosity-temperature relationship in the wall model and DNS can incur significant errors (not shown).

#### 1. Supersonic Channel Flow at cold wall conditions

We first consider the cold wall supersonic channel flow corresponding to the DNS of Coleman et al. [26]. The Mach number ($M_b$) based on the bulk velocity and wall temperature is 1.5 and 3.0, while the Reynolds number based on the bulk density and velocity, and wall viscosity ($Re = \rho_b u_b h/\mu_w$) is 3000 and 4880, respectively. The centerline temperature ($T_c/T_w$) is 1.378 and 2.49 for Mach 1.5 and Mach 3 flows, respectively. The effect of the damping function scalings discussed in Section II A is shown in Figure 5 for the JK mixing-length model. The errors in skin friction ($C_f$) and heat-transfer parameter ($B_q$) are shown for Mach 1.5 and 3.0. For the Mach 1.5 case, we see that overall, the local scaling works best followed by the mixed2 and semilocal scalings. For the Mach 3 flow, the mixed2 scaling works best for both $C_f$ and $B_q$, followed by the semilocal scaling. The SA damping function also works well for these flows, and behaves similar to the semilocal scaling at larger exchange locations. The wall scaling yields the most erroneous results among all the scalings for both the flows, with semilocal giving improved predictions, consistent with previous findings of Bocquet et al. [11] and Yang & Lv [16]. The errors for the two flows are consistent with the values previously reported by Bocquet et al. [11], who used a Prandtl mixing length model instead. Note that the Mach 3 flow has a higher $B_q$ and a colder wall compared to Mach 1.5. Thus, for strongly cooled walls, the mixed2 scaling appears to work best. One can observe a monotonic trend in the errors as we go from the wall, mixed, semilocal, mixed2 and local scalings; with the mixed, mixed2 and semilocal scalings lying between the wall and local scalings. For cold wall flows, $y^+_{wall} > y^+_{SL}$, and so the wall scaling implies lesser damping which yields an overprediction in $C_f$. This is consistent with the behavior observed in the incompressible channel in Figure 1 where an overprediction in $C_f$ was observed for smaller values of $A^+$ (or larger values of $y^+/A^+$). We see that using an incorrect scaling for the damping function (wall scaling for cold wall flows) can results in significant error in the predictions (up to 100%) which was also shown by Yang & Lv [16] for a supersonic Couette flow. Also, the mixedmin/ mixedmin2 scaling lies right on top of the semilocal/ mixed2 scalings, which is expected for cold-wall cases. We also see that the errors are generally lower at $y/h \approx 0.05$, compared to larger values of $y/h$.

We also consider the cold-wall supersonic channel flow corresponding to the DNS of Modesti & Pirozzoli [29] at $M_b = 1.5$ and $Re_b = 17000$, with identical definitions of the two bulk parameters as before. This case has a significantly higher Reynolds number compared to the Coleman et al. [26] data. The errors in $C_f$ and $B_q$ are shown in Figure 6 (a) and (b), respectively. The results are qualitatively similar to those in Figure 5 with the wall scaling overpredicting by up to 25% in both $C_f$ and $B_q$, and the semilocal, mixed2 and local scalings being least erroneous overall. The results also indicate that the errors are lower in magnitude at higher Reynolds numbers compared to the Mach 1.5 results in Figure 5 (a,b), consistent with the analysis of Yang & Lv [16] for supersonic Couette flow.

#### 2. Supersonic Turbulent Boundary Layer at adiabatic conditions

We now consider the adiabatic supersonic turbulent boundary layer corresponding to the study of Pirozzoli & Bernardini [33, 34] and Bernardini & Pirozzoli [35, 36]. The freestream Mach numbers are 2 and 4, and the corresponding $Re_\tau = u_\tau \delta_{99}/\nu_w$ are 1113 and 398, respectively. The errors in $C_f$ and $T_w$ are shown in Figure 7. As observed for the cold-wall flows, we still see a consistent trend in the $C_f$ prediction as we go from the wall, mixed, semilocal,

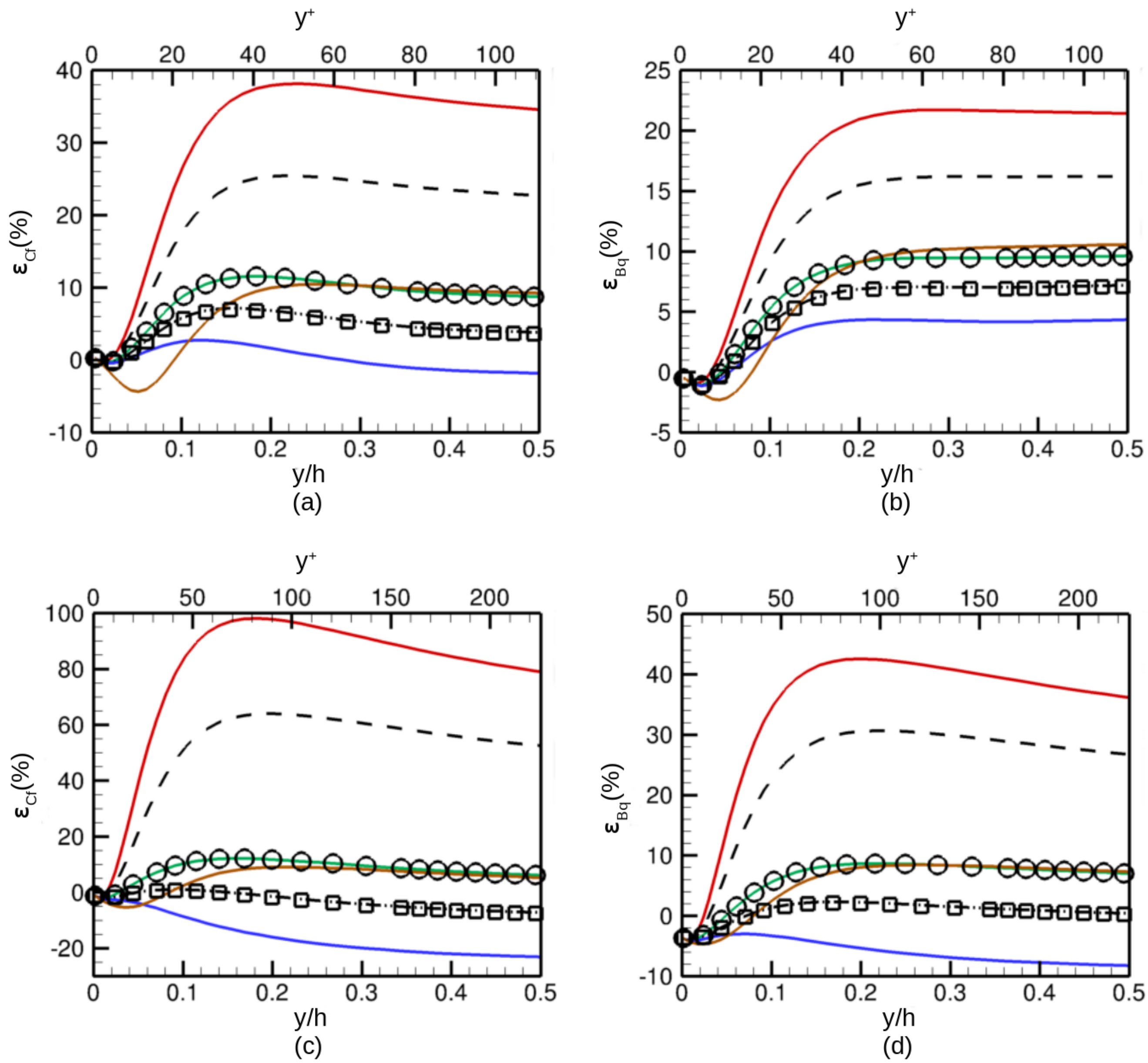


FIG. 5. The effect of damping function scalings is shown for the wall model using the Johnson-King based mixing length model for (a,b) Mach 1.5 and (c,d) Mach 3 cold wall channel flows corresponding to the DNS of Coleman et al. [26]. Legend: ▬ wall, ▬ ▬ mixed, ▬ semilocal, ▬·· mixed2, ▬ local, ▬ SA, ◯ mixedmin and □ mixedmin2.

mixed2 and local scalings. For adiabatic wall flows, $y^+_{wall} < y^+_{SL}$, and so the wall scaling implies more damping which yields an underprediction in $C_f$, while the SL scaling overpredicts $C_f$. In general, the errors are lower for adiabatic walls when compared to cold walls. We see that the mixed scaling best predicts the $C_f$, to within 3% error, while the SA and semilocal damping overpredict the $C_f$ by 5-10% at $y/\delta = 0.1$. The error of the wall and semilocal scalings for adiabatic flows appears to increase with Mach number, as observed between Mach 2 and 4 (and Mach 3 flow, which is not shown here). In terms of the wall temperature predictions, interestingly, the different damping functions have a negligible effect, with all of them predicting nearly identical wall temperature values. The mixedmin and mixedmin2 scalings collapse to the mixed scaling for adiabatic flow, which is most accurate for this regime, compared to the other damping function scalings.

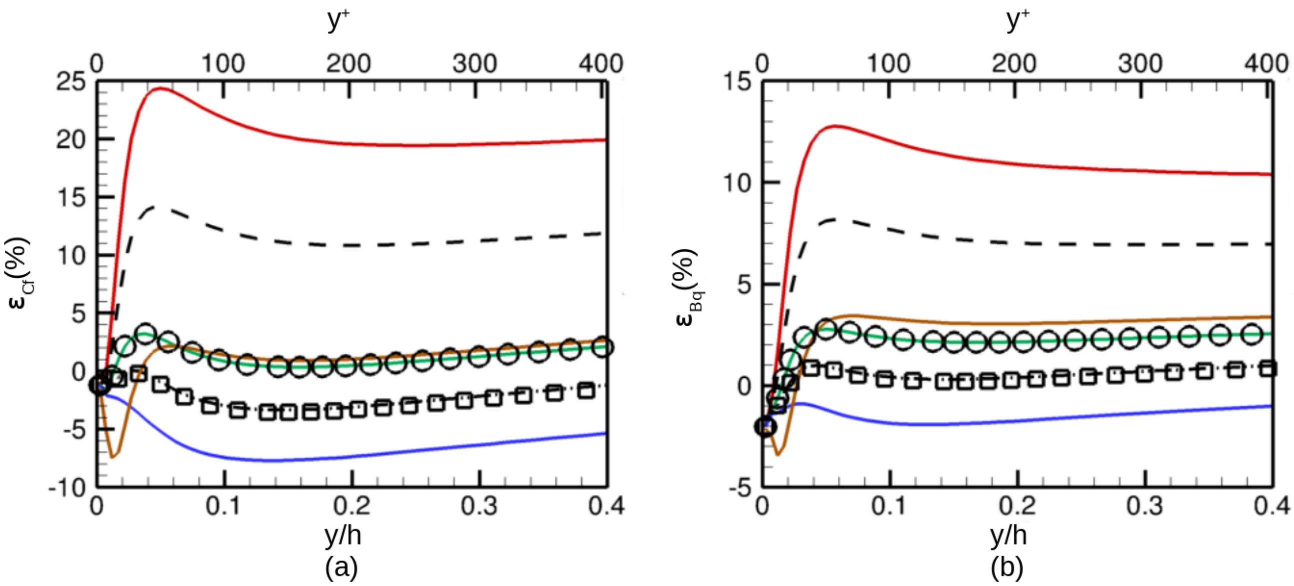


FIG. 6. The effect of damping function scalings is shown for the wall model using the Johnson-King based mixing length model for Mach 1.5 cold wall channel flow for (a) skin friction, and (b) wall heat flux, corresponding to the DNS of Modesti & Pirozzoli [29]. Legend: wall, mixed, semilocal, mixed2, local, SA, ○ mixedmin and □ mixedmin2.

### *3. Hypersonic Turbulent Boundary Layer over a range of thermal conditions*

In this section, the benchmark is the recent turbulent boundary-layer database of Zhang et al. [28], which covers Mach numbers between 2.5 and 14, and wall-temperature conditions from cold through adiabatic conditions. Figure 8(a,b) show the predictions for a Mach 2.5 adiabatic turbulent boundary layer at $Re_\tau = 510$. Generally the findings are similar to those in Section III B 2 in that the mixed (and mixedmin/mixedmin2) scaling give the best prediction overall, with under 2% error for $y/\delta_{99} < 0.1$. The wall scaling too performs well under these conditions. Again, similar to previous observations, the wall-temperature predictions by the different scalings are nearly identical for all the damping function scalings. Figures 8(c,d) show the predictions of errors in $C_f$ and $B_q$ for a Mach 5.86 boundary layer, with $Re_\tau = 453$ and $T_w/T_{ad} = 0.76$, where $T_{ad}$ is the adiabatic recovery temperature. For this case, the wall scaling works best in terms of $C_f$ but is more erroneous for $B_q$. The semilocal, mixed2, local and SA scalings have a significant error in $C_f$ but a lower error in $B_q$. Overall, the mixed scaling works best in terms of both $C_f$ and $B_q$, and the mixedmin and mixedmin2 scalings reduce to the mixed scaling for this flow. But overall, the best predictions have larger errors ($\approx 10\%$) compared to the previous (lower Mach number) cases.

In Figure 9, the errors in $C_f$ and $B_q$ are shown for Mach 7.86 and Mach 13.68 flows, with a corresponding $Re_\tau =$ 480 and 646, and $T_w/T_{ad} = 0.48$ and 0.18. We have so far seen that the wall scaling overpredicted $C_f$ and $B_q$ for cold-wall flows while it underpredicted for adiabatic conditions; thus the errors decrease from cold to adiabatic wall, with the opposite trend (increase in error) for the semilocal scaling. Thus, conceivably there should be a wall condition ($T_w/T_{ad}$) where the semilocal and wall scalings give identical results. It so happens that this occurs for the Mach 7.86 flow for $T_w/T_{ad} = 0.48$, with all the scalings producing nearly identical predictions. However, at $y/\delta = 0.1$, there is significant error of $\approx 20\%$ in $C_f$. Also, at this condition, the mixedmin/ mixedmin2 scalings neither exactly match the mixed or semilocal/ mixed2 scalings, but have slightly lower error overall. This is not unexpected, as the mixedmin/ mixedmin2 scalings were designed to switch between the mixed and semilocal scaling for adiabatic and cold walls. For the Mach 13.68 flow with a cold wall, the results are consistent with previously observed trends for the channel flow of Coleman et al. (Section III B 1). The mixed2 scaling has the least error in $C_f$ overall, and the semilocal and SA scalings have the lowest error in $B_q$. The mixedmin/mixedmin2 scaling matches the semilocal/mixed2 scaling for this condition.

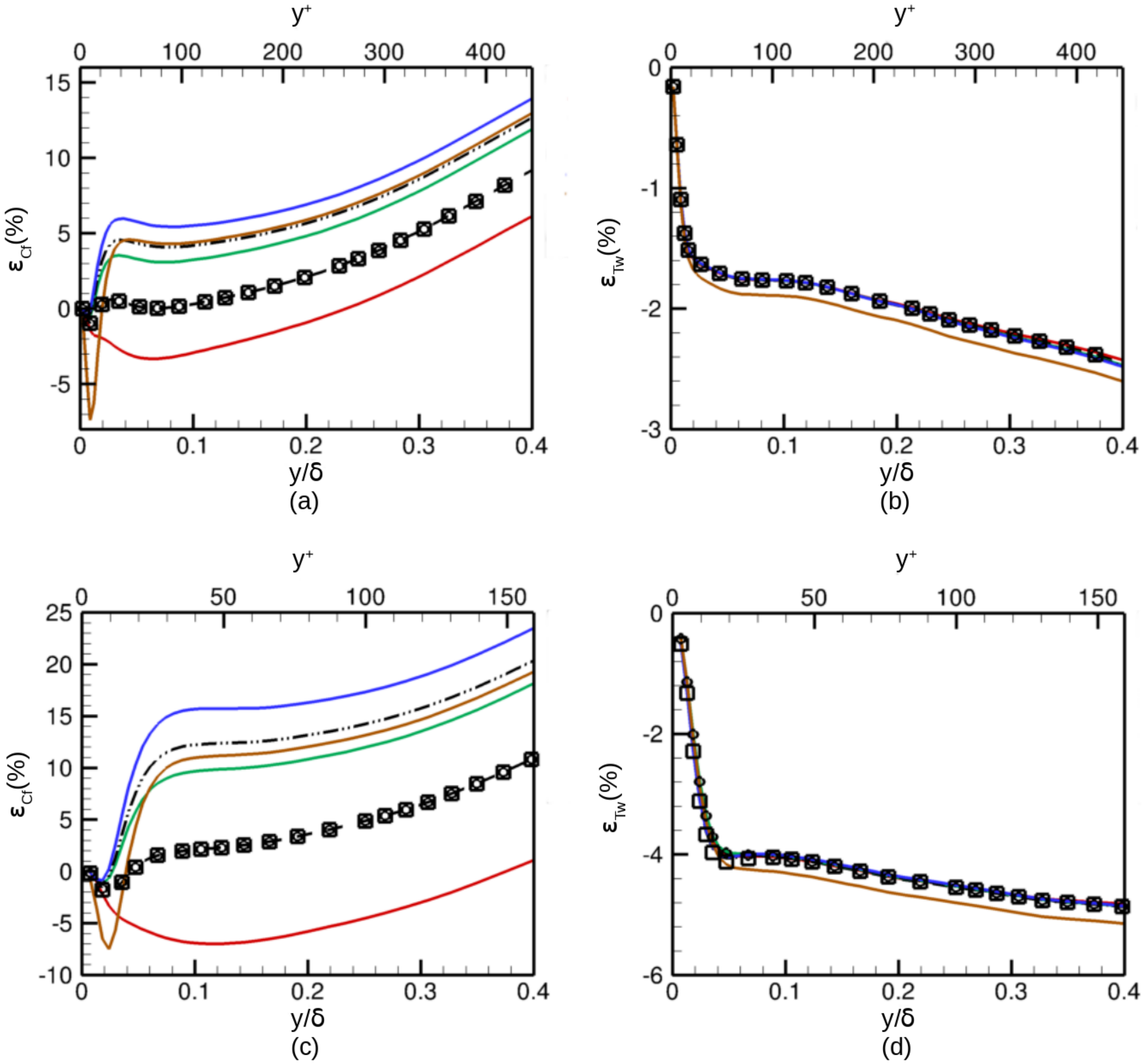


FIG. 7. The effect of damping function scalings is shown for the wall model using the Johnson-King based mixing length model for (a,b) Mach 2 and (c,d) Mach 4 boundary layer at adiabatic conditions. Legend: wall, mixed, semilocal, mixed2, local, SA, ◯ mixedmin and □ mixedmin2.

#### *4. Effect of Mixing-length Model and Turbulent Prandtl Number*

Figure 10 shows the errors in wall quantities, revealing the effect of mixing length model for (a,b) the cold wall Mach 3 channel discussed in Section III B 1 and (c,d) the adiabatic Mach 4 boundary layer discussed in Section III B 2. The Johnson-King based and Prandtl mixing-length models are used. We show results corresponding to the wall and semilocal scalings for the two mixing length models. Note that the damping function is the same for both, with $A^+ = 17$ and 26 for the JK and Pr models respectively based on the previously observed results for incompressible flow (Section III A 1). Similar to observations from incompressible results, we see that the effect of the mixing length model is small for the different flows and scalings shown in the figure. Thus, there appears to be no compelling reason to use one model over another, provided the appropriate value for $A^+$ is used for the damping function.

Figure 11 shows the effect of the turbulent Prandtl number ($Pr_t$) on the wall model errors for (a,b) the Mach 3 cold-wall channel and (c,d) the Mach 4 adiabatic boundary layer. The turbulent Prandtl number is varied between

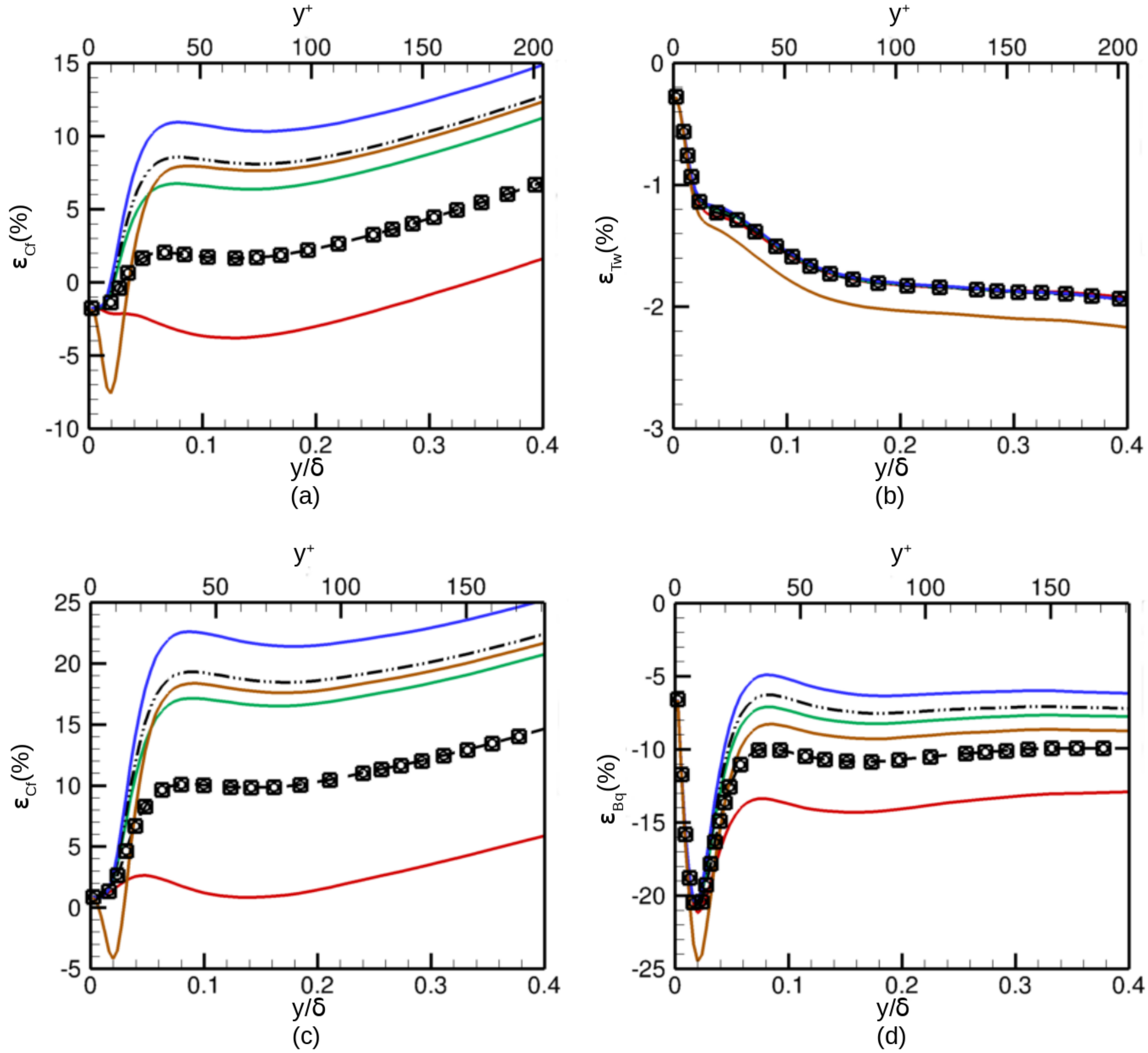


FIG. 8. The effect of damping function scalings is shown for the wall model using the Johnson-King based mixing length model for an (a,b) adiabatic Mach 2.5 and (c,d) Mach 5.86, $T_w/T_{ad} = 0.76$ boundary layer. Legend: wall, mixed, semilocal, mixed2, local, SA, ◯ mixedmin and □ mixedmin2.

0.6 and 2.0. For the channel flow, the influence of $Pr_t$ on the $C_f$ errors appear to be small, but is significant for the errors in $B_q$ with up to 15% variation. For the adiabatic boundary layer flow, the effect of $Pr_t$ on $C_f$ is small until $y/\delta = 0.05$ and significant (up to 20%) beyond that. The turbulent Prandtl number also has a significant effect on the wall temperature prediction for adiabatic flows. Although a large variation in $Pr_t$ was assessed here, typical values of $Pr_t$ are between 0.8 and 1.0. Thus, over this range, the effect of $Pr_t$ may be less significant (under $\approx 5\%$).

### 5. *Quantitative Summary of the A Priori analysis of Damping Function Scaling*

We now summarize the results for the high-speed flows considered so far for the different damping function scalings in Table I. The different cases are named based on the authors of the corresponding reference paper. The accuracy of the results in this table is dependent on the accuracy of the corresponding DNS, which we assume to be the "truth."

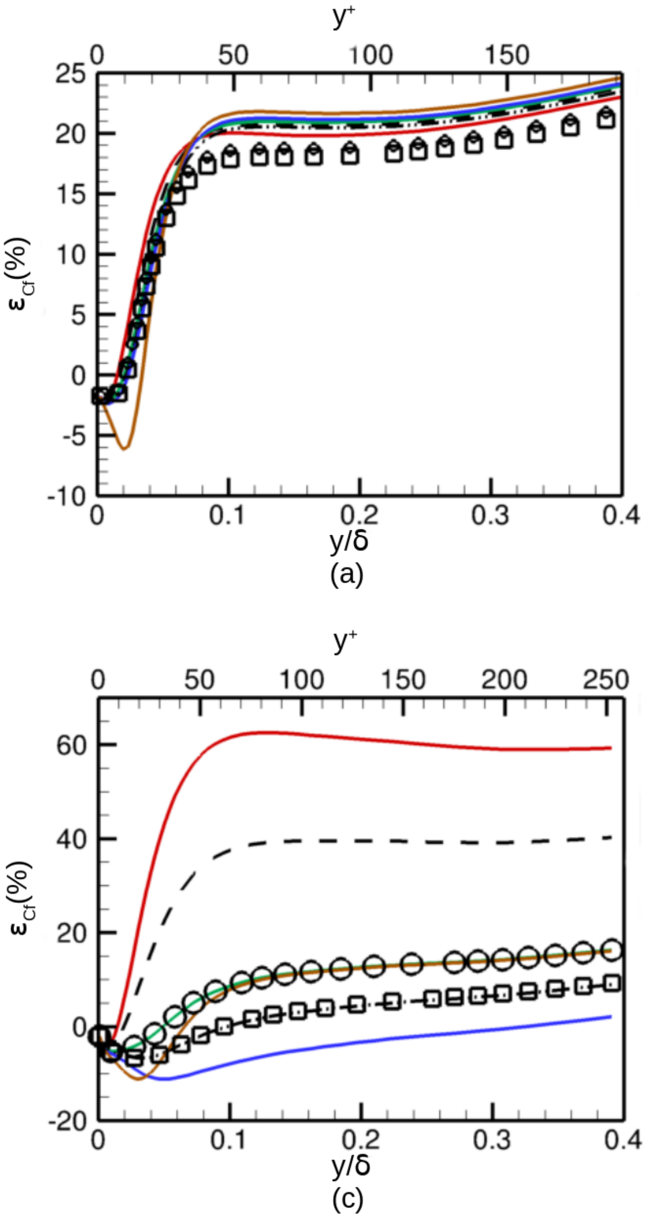


FIG. 9. The effect of damping function scalings is shown for the wall model using the Johnson-King based mixing length model for a (a,b) Mach 7.86, $T_w/T_{ad} = 0.48$ and (c,d) Mach 13.68, $T_w/T_{ad} = 0.18$ boundary layer. Legend: red line wall, dashed line mixed, green line semilocal, dash-dot line mixed2, blue line local, brown line SA, ◯ mixedmin and □ mixedmin2.

The turbulent Prandtl number ($Pr_t$) in the DNS also influences the results, since we have used a value of 0.9 for all the flows in this study. We estimate that the errors due to $Pr_t$ should be small ($< 2\%$), based on the reported values of $Pr_t$ in some of the DNS studies. The value of $T_w/T_{ad}$ reported for the channel flows for comparison with the boundary layer flows is only approximate, and computed based on the centerline temperature $[1 + 0.5r(\gamma - 1)(u_b/\sqrt{\gamma R T_c})^2$ with $r = 0.89]$. Thus, the value of $T_w/T_{ad}$ for internal (channel) and external (boundary layer) flows may not be equivalent.

We report the errors ($\varepsilon_Q\%$) in $C_f$ and $B_q/\ T_w$ at $y/h$ or $y/\delta$ of 5% and 10%, which are the typical exchange locations in WMLES studies. We report the results for the wall, semilocal, local, mixedmin and mixedmin2 scalings for the Van Driest damping function, and the Spalart Allmaras (SA) damping function. The mixed/mixed2 scaling errors are approximately the average of the wall/local and semilocal damping scaling errors as can be observed in Figures 5-9, and so are not reported here. The error values are colored in red, blue and green for error magnitudes $> 10\%$, $5 - 10\%$ and $<= 5\%$, respectively. Our main focus will be on the mixedmin and mixedmin2 scalings, which reduce to the mixed scaling for hot-wall flows, and the semilocal/mixed2 scaling for cold-wall flows.

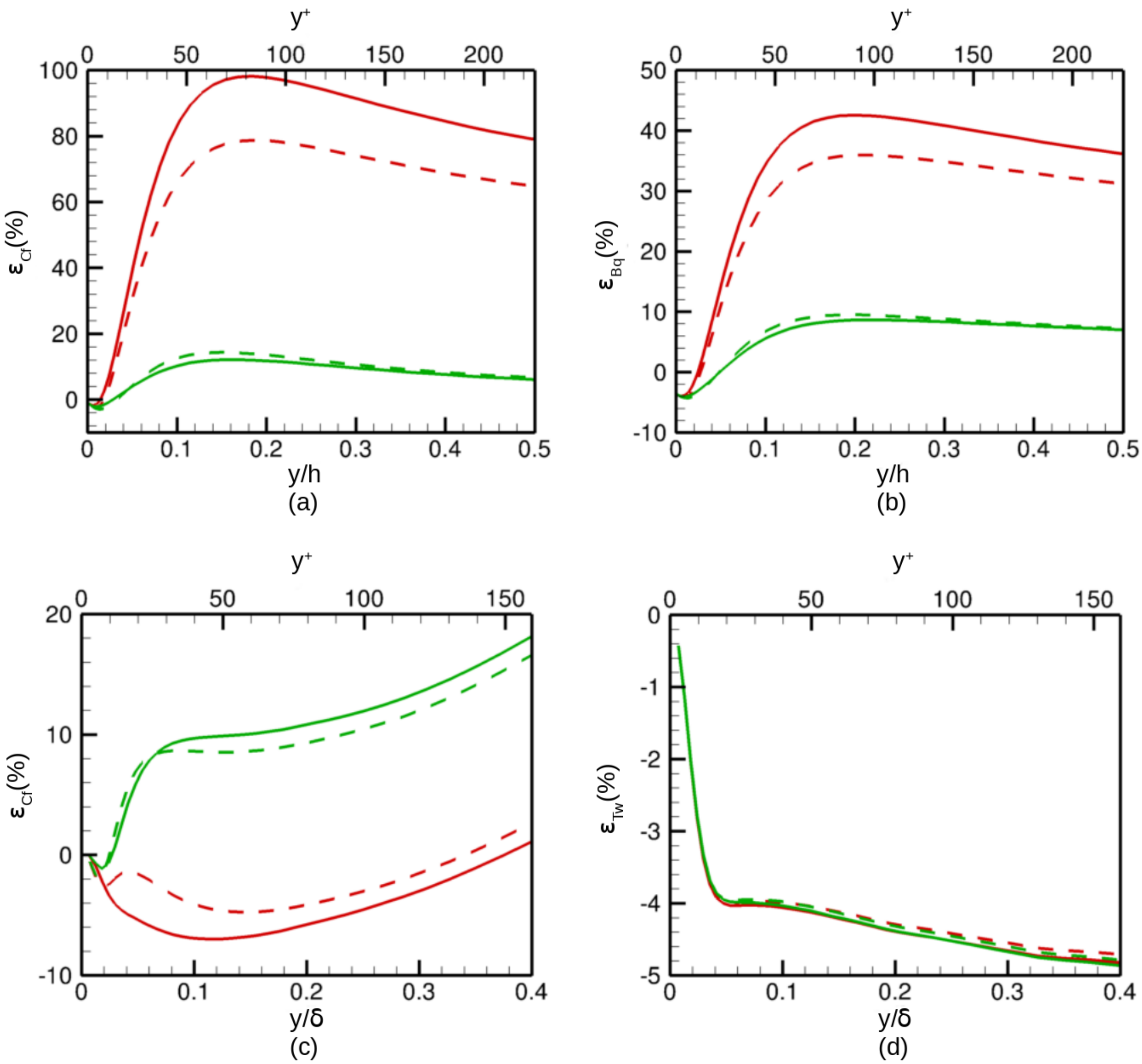


FIG. 10. The effect of mixing length model for (a,b) the cold wall Mach 3 channel flow and (c,d) the adiabatic Mach 4 boundary layer. Legend: ▬ JK wall, ‒ ‒ Prandtl wall, ▬ JK semilocal, ‒ ‒ Prandtl semilocal.

For the cold-wall channel flows corresponding to the DNS of Coleman et al. [26] (CKM) and Modesti & Pirozzoli [29] (MP), we see that at an exchange location of 0.05, both the mixedmin and mixedmin2 give errors under 5%, but at an exchange location of 0.1, the mixedmin2 scaling gives significantly improved predictions. The SA damping function also gives excellent results for cold-wall channel flows, with under 5% error. The wall and mixed scalings give large errors (up to 83%) for these cold wall flows.

For the adiabatic boundary-layer flows corresponding to the DNS of Pirozzoli & Bernardini [33, 34], Bernardini & Pirozzoli [35, 36] (PB) and the Zhang et al. [28] (ZDC) we see that the mixedmin and mixedmin2 scalings give the best predictions overall, with under 5% in both $C_f$ and $T_w$, at both exchange locations. Note that both these scalings reduce to the mixed scaling at this condition. The semilocal and SA scalings generally have higher errors, which increase from 3-4% for Mach 2 to 8-10% for Mach 4. Presumably, based on this trend, the errors would be even higher for hypersonic flows ($M_\infty > 5$).

For the Mach 5.86 boundary layer with $T_w/T_{ad} = 0.25$, and the Mach 13.86 boundary layer with $T_w/T_{ad} = 0.18$ corresponding to Zhang et al. [28], the behavior is generally consistent with the cold-wall channel flows, with the

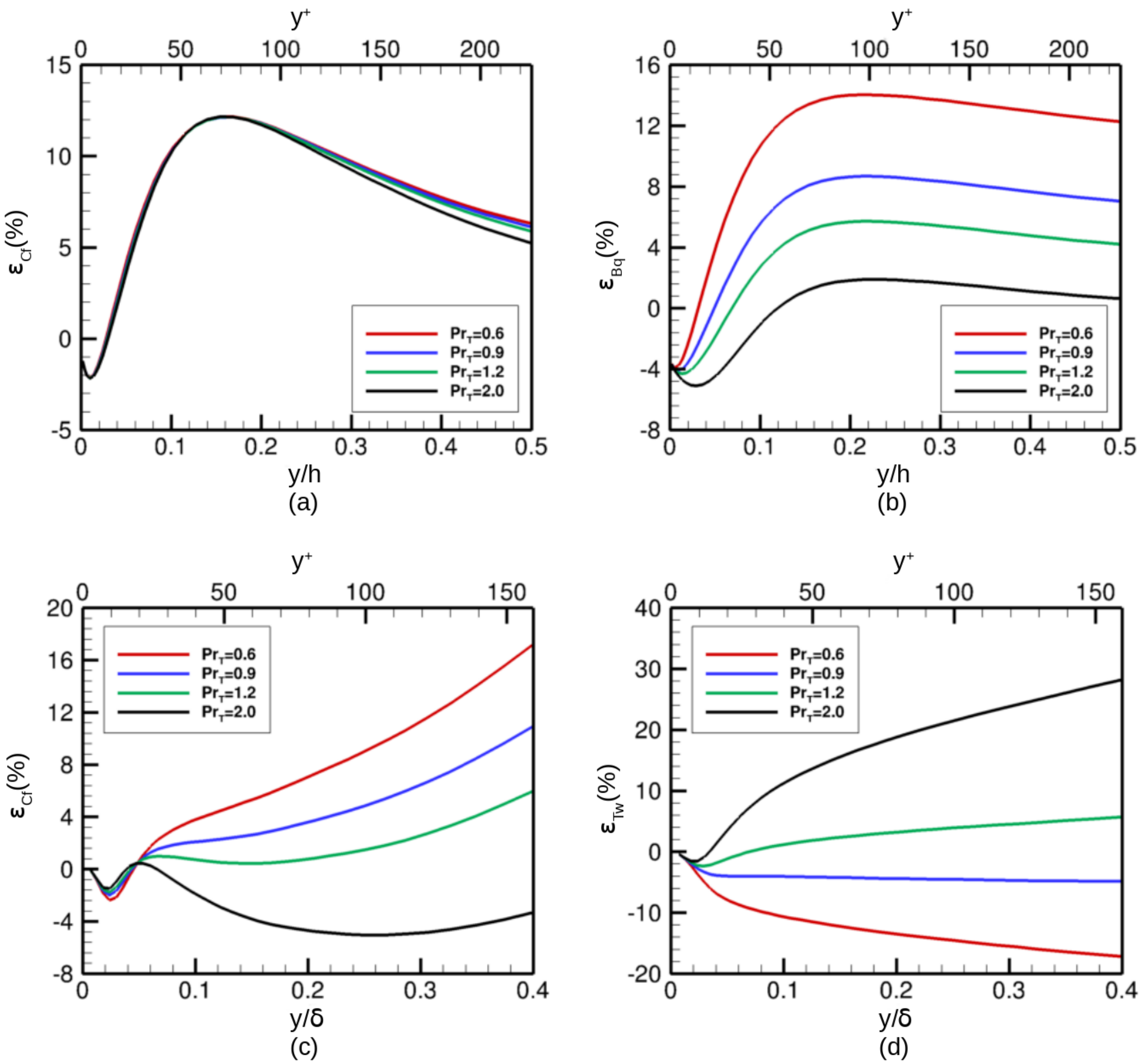


FIG. 11. The effect of turbulent Prandtl number is shown for the wall model using the Johnson-King based mixing length model for (a,b) the cold wall Mach 3 channel flow and (c,d) the adiabatic Mach 4 boundary layer.

mixedmin2 scaling giving the lowest errors overall at both exchange locations. However, we see that the errors in $B_q$ are slightly higher (5-11%) for both the mixedmin and mixedmin2 scalings, which reduce to the semilocal and mixed2 scalings, respectively. The performance of the SA damping function is similar to the semilocal scaling for these flows, with the wall scaling having large errors of up to 62%.

The Mach 5.86 boundary layer with $T_w/T_{ad} = 0.76$ and the Mach 7.86 boundary layer with $T_w/T_{ad} = 0.48$ corresponding to the DNS of Zhang et al. [28] overall have the largest errors for both the mixedmin and mixedmin2 scalings. For the Mach 5.86 case, both the mixedmin and mixedmin2 scalings reduce to the mixed scaling, with an error of up to 12%. For this case, the wall scaling has the minimum error in terms of $C_f$ but has a large error in terms of $B_q$. For the Mach 7.86 flow, we see that all the scalings have similar errors, between 10-20% in terms of $C_f$, but good predictions for $B_q$ with $< 5\%$ error.

Overall, for all the flows, it appears that the mixedmin2 scaling provides the best predictions for both adiabatic and cold wall flows with under 5% error in terms of both $C_f$ and $B_q$ or $T_w$. For intermediate thermal boundary conditions ($T_w/T_{ad} = 0.48, 0.76$), we see that the errors are typically larger, at $\approx 10\%$, at an exchange location of 0.05, and up to 19% at an exchange location of 0.1. We need additional data at these intermediate conditions to attempt to improve the scalings. For the mixedmin scaling, which reduces to the semilocal scaling for cold-wall flows, the errors are generally lower at an exchange location of 0.05 compared to 0.1, but for the mixedmin2 scaling which reduces to the mixed2 scaling, the errors are comparable at both exchange locations.

TABLE I. Errors in prediction of wall quantities ($Q$) at an exchange location ($y/h$ or $y/\delta$) of 0.05, 0.1 are listed using the JK mixing-length model. The errors are highlighted in red, blue and green for error magnitudes $> 10\%$, $5 - 10\%$ and $<= 5\%$, respectively.

| Case | $M$ | $Re_\tau$ | $\frac{T_w}{T_{ad}}$ | $Q$ | wall | SL | local | SA | mixedmin | mixedmin2 |
|---|---|---|---|---|---|---|---|---|---|---|
| CKM [26] | 1.5 | 222 | 0.46 | $C_f$ | 7.9, 26.2 | 2.5, 8.6 | 0.6, 2.5 | -4.3, 1.3 | 2.5, 8.6 | 1.5, 5.6 |
| | | | | $B_q$ | 2.6, 12.9 | 0.4, 5.2 | -0.3, 2.5 | -2.2, 2.4 | 0.4, 5.2 | 0.1, 3.8 |
| | 3.0 | 451 | 0.18 | $C_f$ | 39.2, 83.2 | 3.9, 10.2 | -3.9, -8.6 | -4.8, 2.4 | 3.9, 10.2 | 0.1, 1.1 |
| | | | | $B_q$ | 14.2, 34.4 | 0.1, 5.6 | -3.1, -3.3 | -3.4, 2.4 | 0.1, 5.6 | -1.6, 1.2 |
| MP [29] | 1.5 | 1011 | 0.46 | $C_f$ | 24.4, 21.7 | 2.7, 0.9 | -5.2, -7.4 | 1.9, 1.2 | 2.7, 0.9 | -1.0, -3.0 |
| | | | | $B_q$ | 12.6, 12.0 | 2.7, 2.3 | -1.2, -1.8 | 3.1, 3.3 | 2.7, 2.3 | 0.9, 0.4 |
| PB [33–36] | 2.0 | 1113 | 1.0 | $C_f$ | -3.2, -2.9 | 3.2, 3.3 | 5.7, 5.2 | 4.5, 4.4 | 0.2, 0.3 | 0.2, 0.3 |
| | | | | $T_w$ | -1.7, -1.8 | -1.7, -1.8 | -1.7, -1.8 | -1.9, -1.9 | -1.7, -1.8 | -1.7, -1.8 |
| | 3.0 | 502 | 1.0 | $C_f$ | -4.7, -5.8 | 5.8, 7.1 | 9.9, 11.7 | 5.7, 8.4 | 0.7, 1.1 | 0.7, 1.1 |
| | | | | $T_w$ | -3.4, -3.5 | -3.4, -3.5 | -3.4, -3.5 | -3.6, -3.7 | -3.4, -3.5 | -3.4, -3.5 |
| | 4.0 | 398 | 1.0 | $C_f$ | -5.3, -6.9 | 6.3, 9.7 | 11.0, 15.7 | 5.2, 11.0 | 0.6, 2.1 | 0.6, 2.1 |
| | | | | $T_w$ | -4.0, -4.1 | -4.0, -4.0 | -4.0, -4.0 | -4.2, -4.3 | -4.0, -4.1 | -4.0, -4.1 |
| ZDC [28] | 2.5 | 510 | 1.0 | $C_f$ | -2.2, -2.6 | 5.8, 7.2 | 9.2, 11.1 | 5.5, 8.6 | 1.9, 2.5 | 1.9, 2.5 |
| | | | | $T_w$ | -3.0, -4.4 | -3.0, -4.4 | -3.0, -4.4 | -3.0, -4.4 | -3.0, -4.4 | -3.0, -4.4 |
| | 5.86 | 450 | 0.25 | $C_f$ | 33.3, 59.5 | 2.3, 9.5 | -4.2, -3.1 | -5.8, 6.7 | 2.3, 9.5 | -1.0, 3.2 |
| | | | | $B_q$ | 6.8, 18.9 | -6.2, -1.1 | -9.1, -7.0 | -9.7, -2.3 | -6.2, -1.2 | -7.6, -4.1 |
| | 5.86 | 453 | 0.76 | $C_f$ | 2.7, 1.3 | 14.0, 17.1 | 18.6, 22.5 | 13.6, 18.3 | 8.5, 10.1 | 8.5, 10.1 |
| | | | | $B_q$ | -14.0, -12.9 | -8.9, -6.5 | -7.0, -4.4 | -10.6, -7.5 | -11.3, -9.4 | -11.3, -9.4 |
| | 7.86 | 480 | 0.48 | $C_f$ | 16.2, 20.1 | 13.7, 20.7 | 13.0, 21.0 | 11.9, 21.6 | 12.9, 18.6 | 12.3, 17.7 |
| | | | | $B_q$ | -1.7, 2.0 | -2.9, 2.4 | -3.2, 2.1 | -3.9, 2.1 | -3.2, 1.2 | -3.6, 0.1 |
| | 13.86 | 646 | 0.18 | $C_f$ | 43.2, 61.5 | 0.2, 8.6 | -11.1, -8.0 | -6.1, 7.8 | 0.2, 8.6 | -5.0, 0.3 |
| | | | | $B_q$ | 9.3, 18.2 | -8.4, -2.6 | -13.7, -10.4 | -11.1, -2.9 | -8.4, -2.6 | -11.0, -6.5 |

## IV. *A POSTERIORI* WMLES

So far we have performed *a priori* analysis of wall-model prediction capabilities using the time-averaged DNS databases to identify the most suitable damping function scaling for compressible flows. We now perform *a posteriori* WMLES for a cold wall Mach 3 channel flow and an axisymmetric Mach 2.85 boundary layer. The Johnson-King mixing length model, and the Van Driest damping function with different scalings are used in the wall model. The Charles solver[2] is used in the simulations. This code solves the compressible Navier-Stokes equations on unstructured grids by using a cell-centered finite-volume methodology. The solver is second-order accurate in space for unstructured grids. An explicit third-order Runge-Kutta scheme is used for time advancement. The constant coefficient Vreman model was used to model the subgrid terms. The solver uses an ENO-based reconstruction scheme with an HLLC flux for shock capturing. Further details about the numerics can be found in Khaligi et al. [38]. The solver has been applied to a wide range of problems such as shock/turbulence interaction [12], supersonic jets [39] and WMLES of turbulent separated flows [40–45].

[2] Cascade Technologies, Webpage: `http://www.cascadetechnologies.com` [Last accessed: January 10, 2018]

### A. Supersonic Cold-Wall Channel Flow

We perform WMLES for a supersonic cold wall channel flow corresponding to the DNS of Coleman et al. [26]. The bulk Mach number ($M_b = u_b/c_w$), and the bulk Reynolds number ($Re_b = \rho_b u_b h/\mu_w$) are 3 and 4880, respectively, while the friction Reynolds number ($Re_\tau = u_\tau h/\nu_w$) is 451. Isothermal conditions are imposed at the wall with $T_w/T_b = 0.4186$. The domain size ($L_x/h, L_y/h, L_z/h$) used is (16, 2, 6), with uniform spacings in all three directions using 16 points per channel half width ($h$). The corresponding grid spacings in viscous wall units are $\Delta x^+ = \Delta y^+ = \Delta z^+ = 28$. Periodic boundary conditions were imposed in the streamwise and spanwise directions, while the shear stress and heat flux from the wall model were imposed at the top and bottom walls. The exchange location (EL) at which data was input to the wall model was $y/h = 0.1$ ($y^+ \approx 45$) which corresponds to the second grid point from the wall to minimize numerical/subgrid scale errors based on the reasoning of Kawai & Larsson [10]. The simulation was driven by a source term in the $x$-momentum and energy equations to maintain constant bulk velocity and temperature, respectively. The source terms used were identical to previous WMLES of Bocquet et al. [11], and so the details are not repeated here.

Table II shows the errors in $C_f$ and $B_q$ for the different damping function scalings. Note that the mixedmin/mixedmin2 scaling results are identical to semilocal/mixed2 results for this flow condition. Overall, it can be seen that the results are qualitatively similar to the *a priori* analysis results with the mixedmin2/mixed2 scalings yielding the best predictions with under 2% error at an exchange location of $y/h = 0.1$. Note that the *a priori* and *a posteriori* results are not quantitatively identical, due to other errors in the WMLES as also observed by Bocquet et al. [11]. However, our results are closer to the *a priori* results compared to Bocquet et al. [11], since the exchange location is further away from the wall. We also performed additional simulations for the wall and semilocal scalings using a finer grid, with twice the resolution in each direction, and the results did not vary significantly.

TABLE II. *A Priori* and *A Posteriori* errors ($\varepsilon_Q$%) in $C_f$, $B_q$ for the Mach 3 cold-wall channel flow.

| Case | $y/h\|_{EL}$ | wall | mixed | mixedmin, semilocal | mixedmin2, mixed2 |
|---|---|---|---|---|---|
| *A Priori* | 0.1 | 83.2, 34.4 | 51.0, 22.6 | 10.2, 5.6 | 0.7, 1.2 |
| *A Posteriori* | 0.1 | 68.6, 29.1 | 43.4, 19.6 | 9.3, 5.3 | 0.9, 1.4 |

Figure 12 shows the variation of the time-averaged velocity, temperature and total turbulent shear stress (modeled plus resolved) with the wall-normal coordinate ($y$), and velocity in inner units, for the different damping function scalings used, and is compared with the DNS results. Since we are imposing the bulk velocity and temperature in the simulation, the velocity and temperature when scaled with the bulk quantities are nearly identical for all the damping function scalings, and match well with DNS. Errors up to 5% in the velocity and temperature are expected based on the corresponding errors in the wall quantities from the *a priori* analysis. The turbulent shear stress $\overline{u'v'}$ is best predicted by the mixedmin2/mixed2 scalings. Likewise, when plotted in inner units ($u^+ = u/u_\tau$), the semilocal and mixed2 scalings agree well with DNS, while the mixed and wall scalings show a large error due to the erroneous $C_f$ predicted. Overall, the mixedmin2 scaling yields the best predictions.

### B. Axisymmetric Supersonic Boundary Layer at Adiabatic conditions

We next simulate an axisymmetric supersonic boundary layer interacting with a compression corner corresponding to the experimental conditions of Dunagan et al. [46]. The freestream Mach number ($M_\infty$) is 2.85, and the freestream unit Reynolds number ($Re = \rho_\infty u_\infty/\mu_\infty$) is 18 million/m. This corresponds to an $Re_\theta = \rho_\infty u_\infty \theta/\mu_\infty \approx 12000$ at a station 4.5 cm upstream of the compression corner. We simulate a portion of the experimental domain with an azimuthal extent of 30°. The inflow of the computational domain is 30 cm upstream of the compression corner where the boundary layer thickness $\delta_{in} \approx 0.8$ cm. The grid contained about 22 points per $\delta_{in}$ in the streamwise and wall-normal directions, and 50 points per $\delta_{in}$ in the spanwise direction, with a total grid count of 2 million. The corresponding grid spacings in viscous wall units are $\Delta x^+ = \Delta y_w^+ = 50$ and $\Delta z^+ = 20$ at 4.5 cm upstream of the compression corner. The mean velocity, temperature and turbulent stresses at the inflow were specified using SA-RANS, and a synthetic inflow-turbulence generator based on the method of Shur et al. [47] was used to generate fluctuations at the inflow plane. More details about the computational setup can be found in Iyer & Malik [45]. The

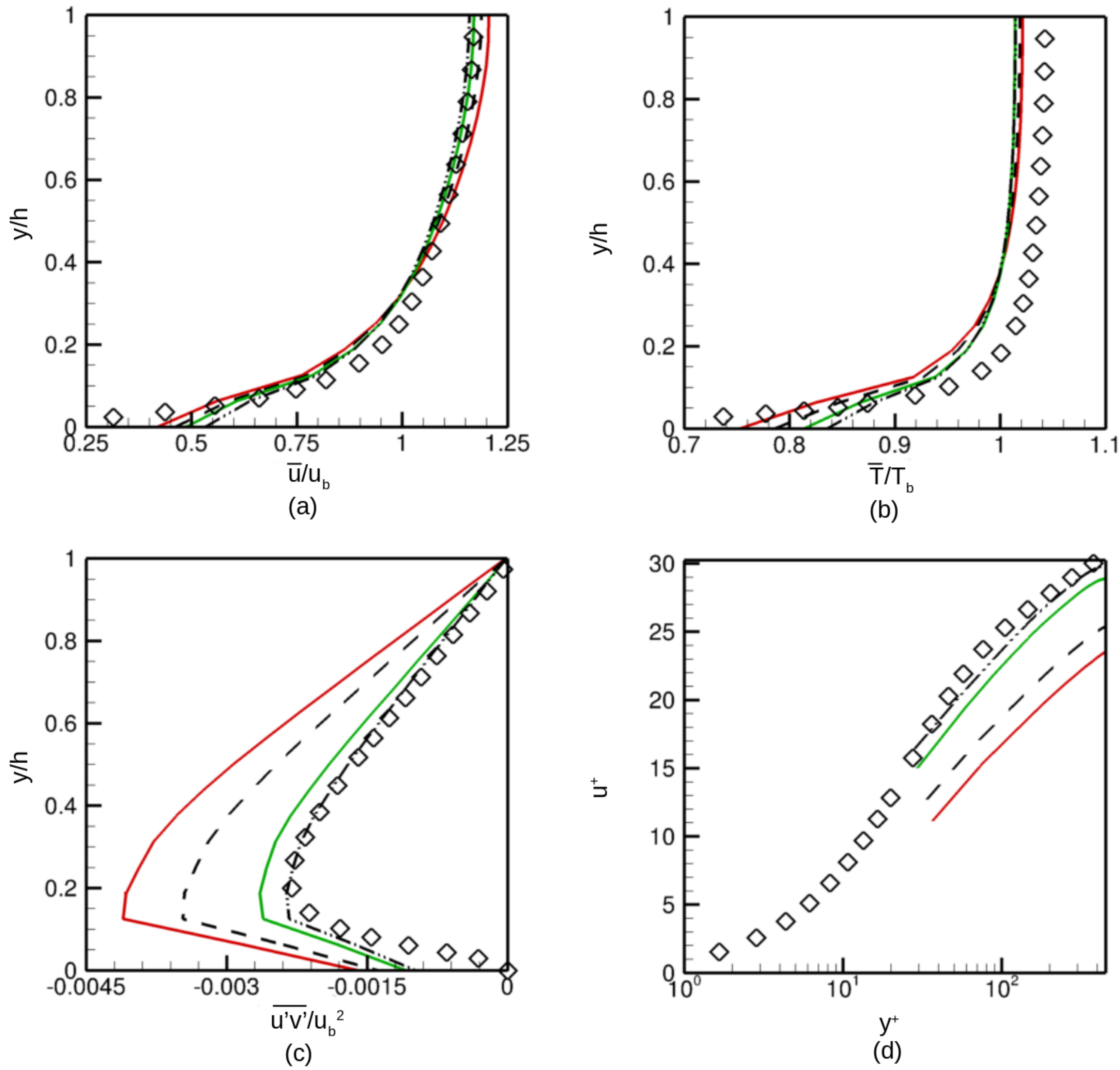


FIG. 12. The variation of (a) time-averaged velocity $(u/u_b)$, (b) temperature $(T/T_b)$, (c) turbulent shear stress $(\overline{u'v'}/u_b^2)$ and (d) velocity in inner units $(u^+)$ for different damping function scalings is shown for the Mach 3 channel flow. Legend: wall, mixed, semilocal/mixedmin, mixed2/mixedmin2, and ⋄ DNS of Coleman et al. [26].

WMLES results were relatively insensitive to the grid resolution in the attached portion of the domain, and to an increase in the azimuthal domain size to 90° [45]. Hence, we will only discuss the results for the coarse grid here.

The *a priori* and *a posteriori* errors at 25 cm from the inflow plane $(x/\delta_{in} \approx 31)$ are reported in Table III for the wall, mixed and semilocal scalings, and are consistent with previous adiabatic results in Table I. The *a priori* analysis was performed using the SA-RANS mean flow data. Note that the mixed2 scaling result is worse than semilocal and so is not shown, and the mixed and mixedmin scalings are identical to the mixedmin2 scaling under this condition. The mixedmin2 scaling gives the best results overall, although the errors in the wall and semilocal scalings are small at this $M_\infty$ and $Re_\theta$. It is interesting that although the mean flow specified was from SA-RANS, the *a priori* analysis did not show any bias towards the semilocal scaling which was closest to the SA damping function, as observed in the previous section. The variation of $C_f$ upstream of the compression corner is shown in Figure 13. The inflow plane is located 30 cm upstream of the compression corner, and the inflow boundary layer thickness $(\delta_{99})$ was 0.8 cm.

Overall, we see that the mixedmin2 scaling agrees best with the SA-RANS result although the errors in the other scalings are small. A transient region associated with the inflow turbulence generation can be observed in Figure 13 until $x/\delta_{in} \approx 20$, indicated by a drop in $C_f$.

TABLE III. *A Priori* and *A Posteriori* errors in $C_f$ and $T_w$ for Mach 2.85 adiabatic axisymmetric boundary-layer flow.

| Case | $y/\delta\|_{EL}$ | wall | semilocal | mixedmin2, mixedmin, mixed |
|---|---|---|---|---|
| *A Priori* | 0.08 | -5.6, 0.03 | 3.6, 0.03 | -0.74, 0.03 |
| *A Posteriori* | 0.08 | -2.2, -0.18 | 4.3, 0.22 | 1.9, -0.17 |

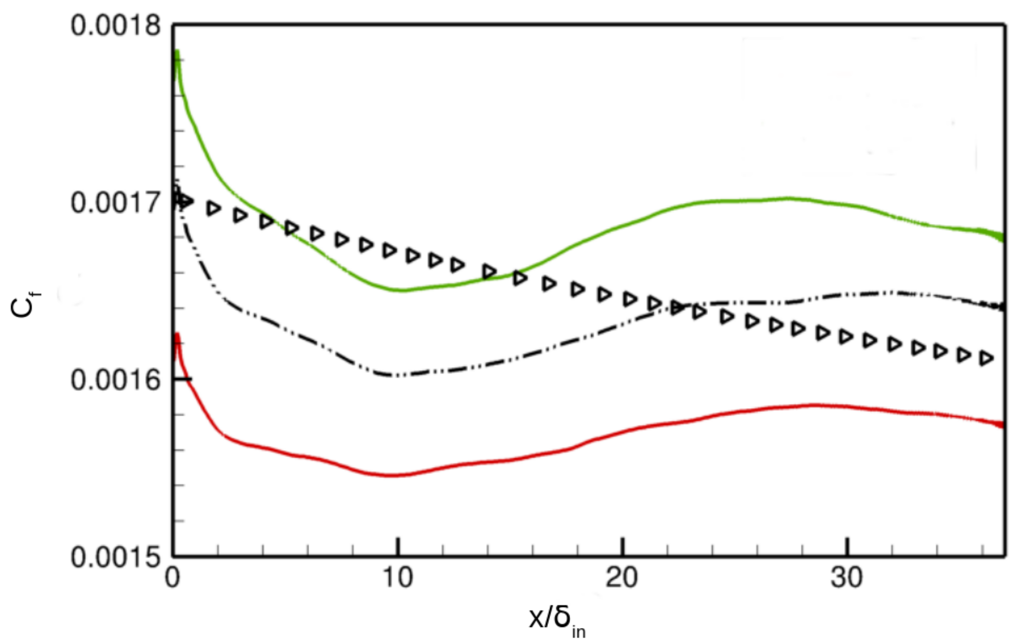


FIG. 13. Variation of $C_f$ in the zero pressure gradient region upstream of the compression corner for the different damping function scalings. Legend: wall, mixed/mixedmin/mixedmin2, semilocal, and $\triangleright$ SA-RANS.

Figure 14 shows the wall normal variation of $\overline{u}/u_\infty$, $\overline{u'v'}/u_\infty^2$ and velocity in inner units ($u^+$) at $x$ =-4.5 cm, and $\overline{\rho}/\rho_\infty$ at $x$ =-5.03 cm. These were the locations at which experimental data were available. Similar to the results for the channel flow, we see that when the quantities are scaled with the outer units (freestream values), the velocity and density profiles are nearly identical for all the scalings. Some differences show up in the turbulent shear stress, which typically scales in inner units ($u_\tau$). Also, in the $\overline{u'v'}$ profiles it can be seen that the results are erroneous very near the wall, due to the coarse wall-normal resolution ($\Delta y_w^+ = 50$) used. The velocity variation in the inner units shows that the mixedmin2 scaling is closest to the SA-RANS. Overall, the agreement with experiment is good, but the results are closer to the SA-RANS results since this was used to provide the mean flow for the inflow turbulence generator.

## V. CONCLUSIONS

We analyzed the predictive ability of an equilibrium wall model for high-speed wall-bounded turbulent flows using *a priori* and *a posteriori* analyses. For the *a priori* analysis, the time-averaged flow parameters from various DNS databases were used as input to the wall model to assess the accuracy of the outputs with respect to the values

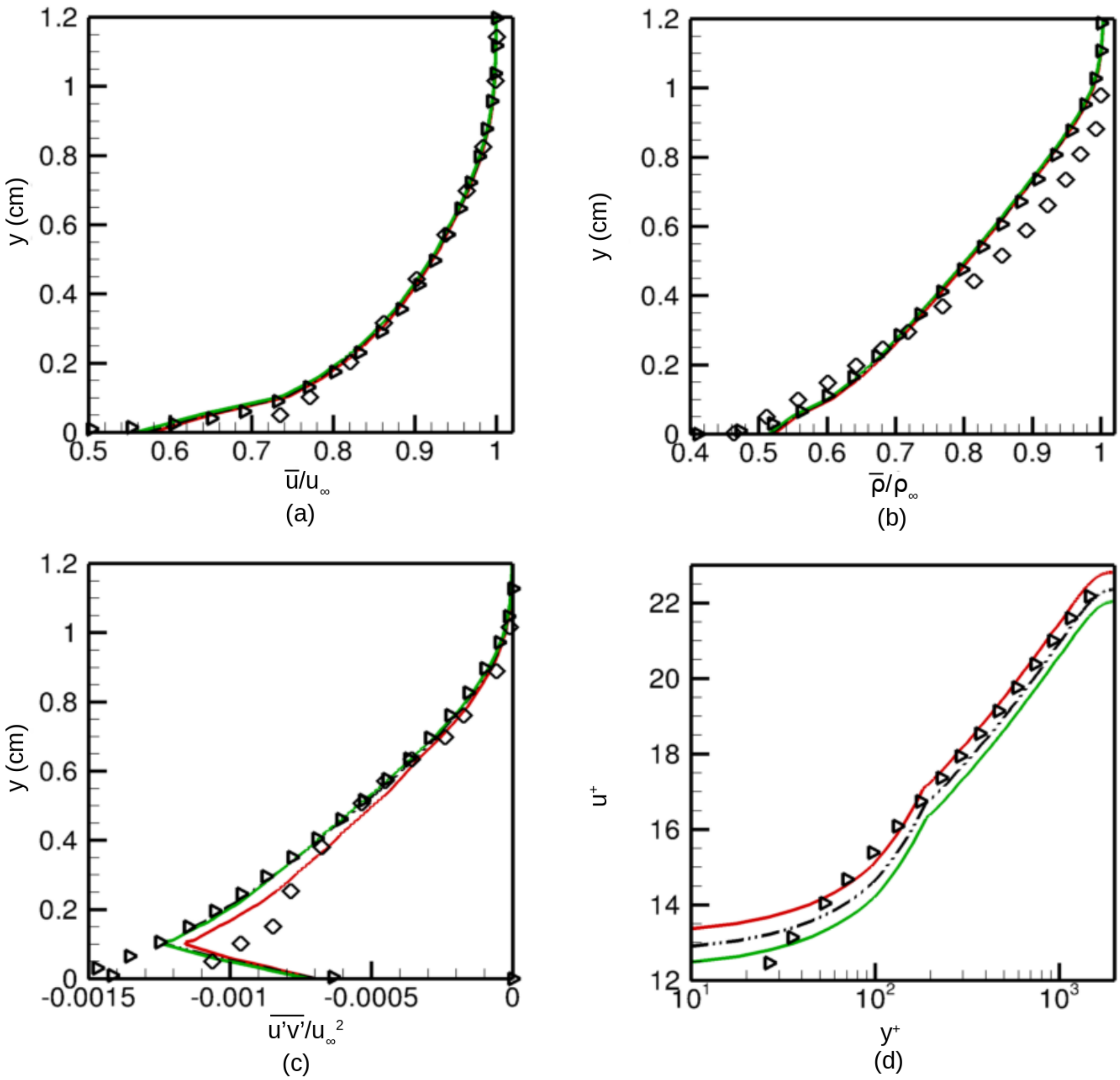


FIG. 14. The variation of time-averaged (a) velocity ($u/u_\infty$), (b) density ($\rho/\rho_\infty$), (c) turbulent shear stress ($\overline{u'v'}/u_\infty^2$) and (d) velocity in inner units ($u^+$) is shown for different damping function scalings for the Mach 2.85 boundary layer flow at $x/\delta_{in} \approx 31$. Legend: wall, mixed/ mixedmin/ mixedmin2, semilocal, $\triangleright$ SA-RANS and $\diamond$ Experiments of Dunagan et al. [46].

obtained from DNS. Two mixing-length models and multiple damping function scalings for the Van Driest damping function were studied. For the *a priori* analysis, we first looked at incompressible flows to assess the sensitivity of the wall model to various parameters, such as the mixing-length model used, Karman constant ($\kappa$), empirical constant in the damping function ($A^+$), and inclusion of the pressure gradient for channel flows. The results confirmed that the values used in most studies, with $\kappa = 0.41$, $A^+ = 26$ for the Prandtl mixing length model and $A^+ = 17$ for the Johnson-King based zero-equation model were optimal. The predictions of both the mixing-length models were of comparable accuracy. We also looked at multiple damping functions, which include the Van Driest, Spalart-Allmaras-based, and a modified Van Driest type function; again the performance of all were of comparable accuracy. The effect of including the pressure gradient term for channel flows was small when the exchange location was less than 10% of the channel half width. Overall, good predictive accuracy was observed for incompressible flows with under 5% error (and even lesser depending on the exchange location) in predicting $C_f$.

We then assessed the predictive ability for high-speed compressible flows for thermal boundary conditions ranging from cold through adiabatic walls. The optimal values of $\kappa$ and $A^+$ for incompressible flows was used to be consistent. Multiple damping function scalings for the Van Driest damping function was studied which include the wall, mixed, semilocal, mixed2, local, mixedmin and mixedmin2 scalings. All these damping function scalings conform to the basic requirement of the damping function ($D \to 0$ as $y \to 0$, and $D \approx 1$ for $y^+ \gtrsim 30$), and reduce to the incompressible scaling at low speeds. Note that one could instead fix the damping function scaling, and vary the $A^+$ depending on the flow conditions to obtain accurate results. However, this would make the values specific to flow conditions. We instead prefer to use the incompressible values of the empirical constants and come up with a general wall-normal scaling for the damping function that would yield best results irrespective of the flow conditions. The wall and semilocal scalings have been used in previous WMLES studies, with the semilocal scaling yielding better predictions for cold wall flows. We proposed newer damping scalings such as mixed and mixed2, whose predictions lie between the semilocal and either wall or local scalings, respectively. Depending on the thermal boundary condition, $y^+_{wall}$ would be higher (cold walls) or lower (hot walls) than $y^+_{local}$ and $y^+_{SL}$. A higher value of $y^+_{wall}$ implies lower damping, and correspondingly an overprediction in $C_f$. Thus, the wall scaling overpredicted $C_f$ for cold wall flows and underpredicted $C_f$ for adiabatic flows, with the opposite trend for the semilocal/local scalings. The mixed, mixed2 scalings were motivated by empirical observations to reduce errors in the prediction of wall quantities. It was observed that the mixed scaling gave the best predictions for adiabatic conditions in terms of both $C_f$ and $T_w$ with under 5% error in both. Overall, the mixed2 scaling gave the best predictions in terms of both $C_f$ and $B_q$ for cold wall flows with under 5% error in both. The semilocal scalings also gave acceptable predictions for cold wall flows, although the errors were higher at farther exchange locations. The mixedmin/mixedmin2 scalings were designed to automatically switch to the mixed scaling for hot walls, and semilocal/mixed2 scalings for cold walls. For the boundary layer flows with intermediate thermal wall conditions, with $T_w/T_{ad} = 0.48$ and 0.76, the wall model errors were generally higher (10-18%) when compared to cold wall ($T_w/T_{ad} < 0.3$) and adiabatic cases. Note that multiple DNS databases were available and used for the analysis at cold wall and adiabatic condtions, thus providing a higher confidence in the inferences. However, for the intermediate wall-temperature boundary-layer cases, only a single DNS database was available, and so these need to be verified with other studies. We also looked at sensitivity to the mixing length model, and found that similar to incompressible flows, both the mixing length models used were of comparable accuracy. The sensitivity to the turbulent Prandtl number ($Pr_t$) indicated that it is around 5% in terms of $C_f$ and $B_q$ or $T_w$ for values ranging between 0.8 and 1.0. Overall, a value of 0.9 seemed to be a reasonable value to use.

*A posteriori* WMLES were performed for a Mach 3 channel flow with a cold wall, and a Mach 2.85 axisymmetric boundary layer at adiabatic conditions, and the results obtained using different scalings for the Van Driest damping function were qualitatively consistent with the *a priori* analysis performed using DNS databases. The mixedmin2 scaling gave best predictions for both flows in terms of wall quantities ($C_f$, $B_q$ or $T_w$), and in terms of the wall normal variation of the time-averaged velocity (in terms of both inner and outer scalings), temperature (or density) and stresses. Some small quantitative differences were observed between the *a priori* and *a posteriori* results owing to *a posteriori* errors such as discretization and subgrid-scale modelling errors, among others.

Overall, based on the analysis over a range of thermal conditions and Mach numbers, we recommend the Van Driest damping function with the mixedmin2 scaling for compressible flows, and an exchange location close to 10% of the boundary layer thickness ($\delta_{99}$) or channel half width ($h$). The mixedmin2 scaling for the Van-Driest damping function gave consistently lower errors compared to other scalings, typically less than 5% in $C_f$ and $B_q$ or $T_w$ for most of the flows considered in this study. While our focus in this study was on WMLES, the mixedmin2 scaling should be equally applicable to RANS models which use a Van-Driest-type damping function such as the Baldwin-Lomax model [48]. The mixedmin2 scaling was arrived at based on empirical observations in this study, and therefore is by no means a perfect scaling. However, we hope that the trends observed in this study for different scalings would lead to a more theoretically rigourous and accurate scaling in future.

## ACKNOWLEDGMENTS

This research was sponsored by the NASA Transformational Tools and Technologies (TTT) Project of the Transformative Aeronautics Concepts Program under the Aeronautics Research Mission Directorate. The work of the first author was sponsored by NASA under cooperative agreement NNL09AA00A. We thank Cascade Technologies for providing the Charles solver and consultation in use of the code, and Gary Coleman, Ponnampalam Balakumar, Balaji Venkatachari, Chris Rumsey and Steven Bauer for comments on the manuscript.

[1] P. Spalart, W. Jou, M. Strelets, and S. Allmaras, Comments on the feasibility of les for wings, and on a hybrid rans/les approach, Advances in DNS/LES **1**, 4 (1997).
[2] W. Cabot and P. Moin, Approximate wall boundary conditions in the large-eddy simulation of high reynolds number flow, Flow, Turbulence and Combustion **63**, 269 (2000).
[3] U. Piomelli and E. Balaras, Wall-layer models for large-eddy simulations, Annual Review of Fluid Mechanics **34**, 349 (2002).
[4] J. Larsson, S. Kawai, J. Bodart, and I. Bermejo-Moreno, Large eddy simulation with modeled wall-stress: recent progress and future directions, Mechanical Engineering Reviews **3**, 15 (2016).
[5] S. T. Bose and G. I. Park, Wall-modeled large-eddy simulation for complex turbulent flows, Annual Review of Fluid Mechanics **50** (2018).
[6] P. R. Spalart, Detached-eddy simulation, Annual Review of Fluid Mechanics **41**, 181 (2009).
[7] S. Deck, Zonal-detached-eddy simulation of the flow around a high-lift configuration, AIAA Journal **43**, 2372 (2005).
[8] P. R. Spalart, S. Deck, M. Shur, K. Squires, M. K. Strelets, and A. Travin, A new version of detached-eddy simulation, resistant to ambiguous grid densities, Theoretical and Computational Fluid Dynamics **20**, 181 (2006).
[9] M. L. Shur, P. R. Spalart, M. K. Strelets, and A. K. Travin, A hybrid rans-les approach with delayed-des and wall-modelled les capabilities, International Journal of Heat and Fluid Flow **29**, 1638 (2008).
[10] S. Kawai and J. Larsson, Wall-modeling in large eddy simulation: Length scales, grid resolution, and accuracy, Physics of Fluids (1994-present) **24**, 015105 (2012).
[11] S. Bocquet, P. Sagaut, and J. Jouhaud, A compressible wall model for large-eddy simulation with application to prediction of aerothermal quantities, Physics of Fluids **24**, 065103 (2012).
[12] I. Bermejo-Moreno, L. Campo, J. Larsson, J. Bodart, D. Helmer, and J. K. Eaton, Confinement effects in shock wave/turbulent boundary layer interactions through wall-modelled large-eddy simulations, Journal of Fluid Mechanics **758**, 5 (2014).
[13] X. Yang, J. Urzay, S. Bose, and P. Moin, Aerodynamic heating in wall-modeled large-eddy simulation of high-speed flows, AIAA Journal , 731 (2017).
[14] E. V. Driest, On turbulent flow near a wall, Journal of the Aeronautical Sciences **23**, 1007 (1956).
[15] B. Aupoix and S. Viala, Compressible turbulent boundary layer modelling, Transitional and turbulent compressible flows-1995 , 139 (1995).
[16] X. I. Yang and Y. Lv, A semi-locally scaled eddy viscosity formulation for les wall models and flows at high speeds, Theoretical and Computational Fluid Dynamics **32**, 617 (2018).
[17] D. A. Johnson and L. King, A mathematically simple turbulence closure model for attached and separated turbulent boundary layers, AIAA Journal **23**, 1684 (1985).
[18] W. Cabot, Large-eddy simulations with wall models, Annual Research Briefs, Center for Turbulence Research, Stanford University (1995).
[19] L. Prandtl, Bericht uber untersuchungen zur ausgebildeten turbulenz, Zs. angew. Math. Mech. **5**, 136 (1925).
[20] E. V. Driest, Turbulent boundary layer in compressible fluids, Journal of the Aeronautical Sciences **18**, 145 (1951).
[21] P. Bradshaw, Turbulence: the chief outstanding difficulty of our subject, Experiments in Fluids **16**, 203 (1994).
[22] P. Huang, P. Bradshaw, and T. Coakely, Turbulence models for compressible boundary layers, AIAA journal **32**, 735 (1994).
[23] P. R. Spalart and S. R. Allmaras, A one-equation turbulence model for aerodynamic flows, Recherche Aerospatiale **1**, 5 (1994).
[24] G. Mellor and H. Herring, Two methods of calculating turbulent boundary layer behavior based on numerical solutions of the equations of motion, in *Computation of Turbulent Boundary Layers Conference, Stanford, CA, August* (1968) pp. 18–25.
[25] U. Piomelli, J. Ferziger, P. Moin, and J. Kim, New approximate boundary conditions for large eddy simulations of wall-bounded flows, Physics of Fluids A: Fluid Dynamics **1**, 1061 (1989).
[26] G. N. Coleman, J. Kim, and R. Moser, A numerical study of turbulent supersonic isothermal-wall channel flow, Journal of Fluid Mechanics **305**, 159 (1995).
[27] A. Trettel and J. Larsson, Mean velocity scaling for compressible wall turbulence with heat transfer, Physics of Fluids **28**, 026102 (2016).
[28] C. Zhang, L. Duan, and M. M. Choudhari, Direct numerical simulation database for supersonic and hypersonic turbulent boundary layers, AIAA Journal **56**, 4297 (2018).
[29] D. Modesti and S. Pirozzoli, Reynolds and Mach number effects in compressible turbulent channel flow, International Journal of Heat and Fluid Flow **59**, 33 (2016).
[30] R. D. Moser, J. Kim, and N. N. Mansour, Direct numerical simulation of turbulent channel flow up to $Re_\tau = 590$, Physics of Fluids **11**, 943 (1999).
[31] M. Lee and R. D. Moser, Direct numerical simulation of turbulent channel flow up to $Re_\tau \approx 5200$, Journal of Fluid Mechanics **774**, 395 (2015).

[32] G. Eitel-Amor, R. Örlü, and P. Schlatter, Simulation and validation of a spatially evolving turbulent boundary layer up to $Re_\theta$= 8300, International Journal of Heat and Fluid Flow **47**, 57 (2014).
[33] S. Pirozzoli and M. Bernardini, Turbulence in supersonic boundary layers at moderate reynolds number, Journal of Fluid Mechanics **688**, 120 (2011).
[34] S. Pirozzoli and M. Bernardini, Probing high-reynolds-number effects in numerical boundary layers, Physics of Fluids **25**, 021704 (2013).
[35] M. Bernardini and S. Pirozzoli, Wall pressure fluctuations beneath supersonic turbulent boundary layers, Physics of Fluids **23**, 085102 (2011).
[36] M. Bernardini and S. Pirozzoli, Inner/outer layer interactions in turbulent boundary layers: a refined measure for the large-scale amplitude modulation mechanism, Physics of Fluids **23**, 061701 (2011).
[37] A. Lozano-Durán and J. Jiménez, Effect of the computational domain on direct simulations of turbulent channels up to $Re_\tau$= 4200, Physics of Fluids **26**, 011702 (2014).
[38] Y. Khalighi, F. Ham, J. Nichols, S. Lele, and P. Moin, Unstructured large eddy simulation for prediction of noise issued from turbulent jets in various configurations, AIAA Paper 2011-2886 (2011).
[39] G. A. Brès, F. E. Ham, J. W. Nichols, and S. K. Lele, Unstructured large-eddy simulations of supersonic jets, AIAA Journal **55**, 1164 (2017).
[40] P. Balakumar, G. Park, and B. Pierce, DNS, LES, and wall-modeled LES of separating flow over periodic hills, Proceedings of the Summer Program, Center for Turbulence Research, Stanford University (2014).
[41] P. S. Iyer and M. R. Malik, Wall–modeled large eddy simulation of flow over a wall–mounted hump, AIAA Paper 2016–3186 (2016).
[42] P. S. Iyer, G. I. Park, and M. R. Malik, A comparative study of wall models for les of turbulent separated flow, Proceedings of the Summer Program, Center for Turbulence Research, Stanford University (2016).
[43] G. I. Park, Wall-modeled large-eddy simulation of a high Reynolds number separating and reattaching flow, AIAA Journal **55**, 3709 (2017).
[44] P. S. Iyer, G. I. Park, and M. R. Malik, Wall–modeled large eddy simulation of transonic flow over an axisymmetric bump with shock-induced separation, AIAA Paper 2017-3953 (2017).
[45] P. S. Iyer and M. R. Malik, Large-eddy simulation of axisymmetric compression corner flow, AIAA Paper 2018-4031 (2018).
[46] S. E. Dunagan, J. L. Brown, and J. B. Miles, Interferometric data for a shock-wave/boundary-layer interaction, NASA-TM-101008 (1986).
[47] M. L. Shur, P. R. Spalart, M. K. Strelets, and A. K. Travin, Synthetic turbulence generators for rans-les interfaces in zonal simulations of aerodynamic and aeroacoustic problems, Flow, Turbulence and Combustion **93**, 63 (2014).
[48] B. Baldwin and H. Lomax, Thin-layer approximation and algebraic model for separated turbulentflows, AIAA Paper 1978–257 (1978).